European Journal of Cell Biology 103 (2024) 151455

Contents lists available at ScienceDirect

European Journal of Cell Biology

journal homepage: www.elsevier.com/locate/ejcb

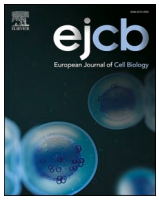

A point-of-research decision in synovial tissue engineering: Mesenchymal stromal cells, tissue derived fibroblast or CTGF-mediated mesenchymal-to-fibroblast transition

Alexandra Damerau [a,b,*], Marieluise Kirchner [c], Philipp Mertins [c], Frank Buttgereit [a,b], Timo Gaber [a,b,*]

[a] Charité – Universitätsmedizin Berlin, corporate member of Freie Universität Berlin and Humboldt-Universität zu Berlin, Department of Rheumatology and Clinical Immunology, Berlin, Germany
[b] German Rheumatism Research Centre (DRFZ) Berlin, a Leibniz Institute, Berlin, Germany
[c] Core Unit Proteomics, Berlin Institute of Health at Charité - Universitätsmedizin Berlin and Max-Delbrück-Center for Molecular Medicine, Berlin, Germany

ARTICLE INFO

Keywords:
Trauma-fibroblast
Osteoarthritis
Metabolism
Cytokines
Synovial membrane model

ABSTRACT

Rheumatoid arthritis (RA) and osteoarthritis (OA) are prevalent inflammatory joint diseases characterized by synovitis, cartilage, and bone destruction. Fibroblast-like synoviocytes (FLSs) of the synovial membrane are a decisive factor in arthritis, making them a target for future therapies. Developing novel strategies targeting FLSs requires advanced *in vitro* joint models that accurately replicate non-diseased joint tissue. This study aims to identify a cell source reflecting physiological synovial fibroblasts. Therefore, we newly compared the phenotype and metabolism of "healthy" knee-derived FLSs from patients with ligament injuries (trauma-FLSs) to mesenchymal stromal cells (MSCs), their native precursors. We differentiated MSCs into fibroblasts using connective tissue growth factor (CTGF) and compared selected protein and gene expression patterns to those obtained from trauma-FLSs and OA-FLSs. Based on these findings, we explored the potential of an MSC-derived synovial tissue model to simulate a chronic inflammatory response akin to that seen in arthritis. We have identified MSCs as a suitable cell source for synovial tissue engineering because, despite metabolic differences, they closely resemble human trauma-derived FLSs. CTGF-mediated differentiation of MSCs increased *HAS2* expression, essential for hyaluronan synthesis. It showed protein expression patterns akin to OA-FLSs, including markers of ECM components and fibrosis, and enzymes leading to a shift in metabolism towards increased fatty acid oxidation. In general, cytokine stimulation of MSCs in a synovial tissue model induced pro-inflammatory and pro-angiogenic gene expression, hyperproliferation, and increased glucose consumption, reflecting cellular response in human arthritis. We conclude that MSCs can serve as a proxy to study physiological synovial processes and inflammatory responses. In addition, CTGF-mediated mesenchymal-to-fibroblast transition resembles OA-FLSs. Thus, we emphasize MSCs as a valuable cell source for tools in preclinical drug screening and their application in tissue engineering.

1. Introduction

Fibroblasts were previously perceived only as mesenchymal lineage cells that form connective tissues and contribute to the structural and positional maintenance of organs, collagen production, extracellular matrix (ECM) synthesis, tissue repair, and, if dysfunctional, fibrosis (Plikus et al., 2021). The latter results from the tissue repair response that becomes dysregulated following many types of tissue injury, most notably during chronic inflammatory disorders. In the meantime, fibroblasts have emerged as multifaceted cells with diverse roles in various tissues, including their critical interactions with immune and inflammatory cells (Chang et al., 2002; Jiang et al., 2023; Lendahl et al., 2022; Plikus et al., 2021). Despite their widespread distribution, the identification of fibroblasts has been oversimplified in the past, often relying on morphological features due to the lack of unique molecular markers (Goodpaster et al., 2007). However, fibroblasts are drivers in

* Corresponding authors at: Charité – Universitätsmedizin Berlin, corporate member of Freie Universität Berlin and Humboldt-Universität zu Berlin, Department of Rheumatology and Clinical Immunology, Berlin, Germany.
E-mail addresses: alexandra.damerau@charite.de (A. Damerau), timo.gaber@charite.de (T. Gaber).

https://doi.org/10.1016/j.ejcb.2024.151455
Received 10 March 2024; Received in revised form 22 August 2024; Accepted 1 September 2024
Available online 10 September 2024

fibrotic diseases such as systemic sclerosis, pulmonary fibrosis, cardiac fibrosis, liver fibrosis, and muscle fibrosis. As cancer-associated fibroblasts, fibroblasts provide a metabolic niche for solid tumors. In age-related chronic inflammatory joint diseases such as autoimmune-mediated rheumatoid arthritis (RA) and degenerative osteoarthritis (OA), fibroblasts located within the synovial membrane become activated and proliferate, covering, invading, and destroying the cartilaginous tissue of the joint. In joint homeostasis, the synovial membrane consists of a lining layer (intima) and sublining layer (subintima), owing to different types of fibroblasts. The intima, which is in direct contact with the synovial fluid-filled joint cavity, plays a crucial role in determining the composition of the synovial fluid by filtering and synthesizing nutrients and lubricants to nourish and lubricate the cartilage (Rhee et al., 2005; Smith, 2011). The intima is composed of one to four cell layers with approximately 90 % fibroblast-like (type B) synoviocytes (FLSs) and 10 % macrophage-like (type A) synoviocytes (MLSs) (Bondeson et al., 2006). In contrast, the sublining layer is a paucicellular connective tissue with fibrous and collagenous ECM and adipose tissue areas with few blood vessels (Scanzello and Goldring, 2012; Smith, 2011). The synovial morphology changes in inflammatory conditions, typical for RA and OA. The synovium thickens to form a pannus-like structure with an increase in cellularity (hyperplasia) due to, e.g., immune cell infiltration, vascularization, fibrosis, and an enhanced innervation, correlating to disease progression and severity (Damerau and Gaber, 2020; Firestein and McInnes, 2017; Smith, 2011; Smolen et al., 2018). Over the last decade, the role of fibroblasts has increasingly emerged as a driving force in the pathogenesis of these diseases, in addition to maintaining joint integrity. They are now recognized as a critical link between synovial inflammation, fibrosis, cartilage degradation, and progressive joint degeneration (Huber et al., 2006; Smith et al., 2023). However, our understanding of how these cells respond to inflammatory and fibrotic stimuli remains limited.

In vitro models have been developed to mimic synovitis, each with advantages and limitations (Baymurat et al., 2015; Broeren et al., 2019; Damerau and Gaber, 2020; Kiener et al., 2010). Synovial explants, for example, preserve the native ECM and spatial distribution of FLSs and MLSs but are limited in availability, especially when obtaining "healthy" clinical samples (Damerau and Gaber, 2020). Instead, clinical specimens are usually obtained from advanced-stage OA patients and are phenotypically and functionally altered due to donor variability in disease state, medication, and biopsy site (de Almeida et al., 2016). In contrast, monolayer cultures lack the dense ECM and complex three-dimensional (3D) architecture that is crucial for the functionality of native tissues. Recently, 3D synovial organoids constructed from micro-mass cultures of RA- or OA-FLSs embedded in animal-derived Matrigel™ have been developed, replicating the ECM-like and cellular features of the intima. It becomes hyperplastic in the presence of inflammatory cytokines (Broeren et al., 2019; Karonitsch et al., 2017; Kiener et al., 2010). However, these models have drawbacks, including the lack of the physiological geometry to facilitate polarized cell migration and solute transport. In addition, FLSs from patients with RA or OA may have an intrinsic imprinted pathological phenotype or be influenced by medication, not reflecting the physiological state of the synovial membrane (Ai et al., 2018; Ge et al., 2021; Shen et al., 2017; Ulukan et al., 2019). Thus, a “normal” or “healthy” FLS source would be ideal for establishing an animal-free 3D synovial membrane model that provides the physiological geometry.

The origin of fibroblasts, particularly those in the synovium, remains the subject of ongoing research and debate. The hypothesis that fibroblasts are derived from epithelial or endothelial cells has been experimentally substantiated in numerous studies on organ fibrosis (Iwano et al., 2002; McAnulty, 2007; Zeisberg and Kalluri, 2004). However, this is not true for all fibroblasts. In addition to stromal cells, fibroblasts function as parenchymal cells, particularly in specialized connective tissues such as ligaments and tendons. The discovery of multipotent mesenchymal cells in tendons (Bi et al., 2007) has fueled the longstanding hypothesis of a mesenchymal origin of fibroblasts (McAnulty, 2007). Recent research indicates that bone marrow-derived MSCs and FLSs are indistinguishable and share numerous features, such as maintaining and regenerating tissues through ECM components and responding to various inflammatory and non-inflammatory factors (Cappellesso-Fleury et al., 2010; Denu et al., 2016a). This similarity extends to their morphology, highly similar surface marker profile, and potential to differentiate into multiple cell lineages, suggesting the assumption of an identical cell type (Blasi et al., 2011; Denu et al., 2016b).

However, the differentiation pathway from MSCs to FLSs is still poorly understood and controversially discussed. Various growth factors, such as connective tissue growth factor (CTGF) (Lee et al., 2006, 2010b; Tong et al., 2011; Yoon et al., 2018), fibroblast growth factor (FGF) (Han et al., 2011; Li et al., 2017), insulin-like growth factor (IGF) (Fan et al., 2008; Moreau et al., 2005), and transforming growth factor (TGF)-β (Bordignon et al., 2019; Li et al., 2017), are capable of promoting the differentiation of MSCs into FLSs. This was evidenced by the expression of classical fibroblast markers, e.g., vimentin (VIM), collagen type I (COL1) fibroblast-specific protein 1 (FSP1), and tenascin-C (TNC) (Lv et al., 2014; Soundararajan and Kannan, 2018). In addition to serum and growth factors, ascorbic acid — commonly known as vitamin C — plays a pivotal role in various cellular functions, notably in enhancing cell proliferation *in vitro*, as well as being essential for the maintenance of connective tissues, the healing of wounds, and the process of scar formation (Ghahremani-Nasab et al., 2023). The pathways through which MSCs differentiate into FLS to maintain and repair connective tissues, especially in response to trauma, cancer, and infection, remain unclear. The main limitation of previous studies is the lack of a suitable fibroblast cell population for comparison. Furthermore, in contrast to other well-studied mesenchymal lineages, e.g., osteoblasts, adipocytes, or chondrocytes, the differentiation pathway from MSCs to FLSs — if one exists — has been poorly defined and is still controversially discussed.

Here, we aimed to identify a cell source reflecting physiological synovial fibroblasts. Therefore, we investigated the effects of CTGF alone, in combination with either FGF or IGF as well as with FGF and IGF together, on the transition of MSCs to FLSs. We compared the phenotypic characteristics of trauma patient-derived FLSs with human bone marrow-derived MSCs and analyzed the proteome of undifferentiated and differentiated MSCs compared to FLSs from OA patients. Finally, we tested the potential of the most appropriate cell type to simulate arthritis in an *in vitro* model.

2. Material and methods

2.1. Cells and ethic statement

MSCs isolation, expansion, adipogenic, osteogenic and chondrogenic differentiation, and characterization were performed as described previously (Damerau et al., 2020). Bone marrow was obtained from patients undergoing total hip replacement, provided by the Center for Musculoskeletal Surgery (Charité–Universitätsmedizin), and distributed by the “Tissue Harvesting” core facility of the Berlin-Brandenburg Center for Regenerative Therapies (BCRT). FLSs were isolated from synovial tissue sections of (i) trauma patients collected during anterior cruciate ligament (ACL) reconstruction and (ii) OA patients excised during knee arthroplasty. Synovial tissue was provided by the Center of Musculoskeletal Surgery (Charité–Universitätsmedizin). The study design and protocols were approved by the Charité-Universitätsmedizin Ethics Committee and performed according to the Helsinki Declaration (ethical approval EA1/012/13, January 2013, EA1/146/21, May 2021).

2.2. Isolation of human synovial fibroblasts

The synovium was washed with 0.5 % (w/v) BSA (Sigma-Aldrich, Munich, Germany) and 5 mM EDTA (Gibco, Waltham, MA, USA) in

phosphate-buffered saline (PBS; DRFZ, Berlin, Germany; PBS/BSA/EDTA; pH 7.4) and dissected into small pieces. The small tissue pieces were filtered through a pre-wetted 100 μm MACS® SmartStrainer (Miltenyi Biotec, Bergisch Gladbach, Germany), transferred to a 25 cm^2 (trauma synovium) or 75 cm^2 flask (OA synovium), and cultured in a humidified atmosphere (37 °C, 5 % CO_2). Dulbecco`s Modified Eagle Minimal Essential Medium (DMEM) GlutaMAX™ (Gibco, Waltham, MA, USA) supplemented with 10 % FCS (FCS, Biowest, Nuaillé, France) and 1 % penicillin/streptomycin (Gibco, Waltham, MA, USA) was changed weekly. This medium is referred to as normal medium (NM).

2.3. Stimulation with growth factors for MSC to fibroblast transition

To differentiate MSCs toward the fibroblast lineage, cells were cultured for three weeks using NM supplemented with (i) 25 ng/mL recombinant human (rh) FGF (ImmunoTools GmbH, Friesoythe, Germany), (ii) 5 and 10 ng/mL rhFGF + rhTGF-β (R&D Systems, Inc., Minneapolis, USA), (iii) 100 ng/mL rhCTGF (PeproTech, Hamburg, Germany) and 50 μg/mL ascorbic acid (Sigma-Aldrich, Munich, Germany), or (iv) unstimulated.

2.4. Flow cytometry analysis

To characterize synovial fibroblasts regarding their surface marker pattern, flow cytometry staining was performed using 5×10^4 cells per well of a U-bottom 96-well plate. After a washing step with PBS/BSA/Azide, unspecific binding sites of the Fc-receptors were blocked using 10 mg/mL Flebogamma® (IgG1 66.6 %, IgG2 28.5 %, IgG3 2.7 %, IgG4 2.2 %; Grifols, Barcelona, Spain) for 10 min on ice. Subsequently, cells were stained with the antibodies according to the manufacturer's instructions (antibodies listed in Table 1). Cells were washed, centrifuged (400 × *g*, 4 min, 4 °C), and suspended in PBS/BSA/Azide. Measurement was performed using the MACSQuant® Analyzer 10 (Miltenyi Biotec, Bergisch Gladbach, Germany) and analyzed with FlowJo™ software (version 7.6.4 and 10.7.1, Tree Star).

2.5. Immunofluorescence staining

Immunofluorescence staining was performed as previously described (Damerau et al., 2020) using target-specific antibodies listed in Table 2. All stainings were conducted in a humid chamber. Imaging was accomplished with the Zeiss LSM 710 Confocal Microscope (Carl Zeiss AG, Oberkochen, Germany).

Table 1
Donor information and conducted experiments.

Description	Dye	Species/ Clone	Manufacturer	City, State
Anti-human CD73	APC	REA804	Miltenyi Biotec	Bergisch Gladbach, Germany
Anti-human CD90	FITC	REA897		
Anti-human CD105	APC-Vio770	REA794		
Anti-human CD14	PE	REA599		
Anti-human CD20	PE	REA780		
Anti-human CD34	PE	REA1164		
Anti-human CD45	PE	REA747		
Anti-human HLA-DR	PE	REA805		

Table 2
List of antibodies, kits, and staining solutions.

Description	Dye	Host	Working concentration	Manufacturer
Immunofluorescence antibodies				
DAPI		-	1 μg/mL	DRFZ
Phalloidin	TRITC	-	50 μg/mL	Sigma-Aldrich
Vimentin	A488	rabbit	5 μg/mL	Abcam
THY1	A568	rabbit	5 μg/mL	
PDPN	-	rat	2.5 μg/mL	BioLegend
anti-mouse IgG (H+L)	A594	goat	2 μg/mL	Abcam
anti-rabbit IgG (H+L)	A488	donkey	4 μg/mL	Invitrogen / Thermo Fisher Scientific
anti-rabbit IgG (H+L)	A546	goat	4 μg/mL	
anti-mouse IgG (H+L)	A546	goat	4 μg/mL	
anti-rat IgG (H+L)	A647	goat	4 μg/mL	
Kits and solutions				
LIVE/DEAD® Viability/ Cytotoxicity	2 μM Calcein AM, 4 μM EthD−1			Invitrogen / Thermo Fisher Scientific
FluoroMount-G™	Mounting slides for immunofluorescence			Sigma-Aldrich
Tween® 20	0.1 % for permeabilization			Qbiogene Inc.

2.6. Seahorse™ technology

Metabolic characterization was performed as described previously (Damerau et al., 2022). Briefly, cells were resuspended in XF assay media (Agilent Technology) supplemented with 10 mM glucose (Sigma-Aldrich), 1 mM pyruvate (Sigma-Aldrich) and 2 mM glutamine (Sigma-Aldrich) and seeded into the Seahorse XF Cell Culture Microplate (Agilent Technology). The Mito Stress Test was performed using 2 μM oligomycin, 1.5 μM FCCP (carbonyl cyanide-p-trifluoromethox-yphenyl-hydrazon), 0.5 μM rotenone and 0.5 μM antimycin A (RotAA). The Glycolytic Rate Test was performed using 0.5 μM RotAA and 50 mM 2-Deoxy-D-glucose. Mitochondrial stress and glycolytic parameters were measured via OCR in pmol/min/1×10^5 cells and PER in pmol/min/1×10^5 cells.

2.7. Protein isolation and mass spectrometry (LC-MS/MS)

Protein isolation and mass spectrometry from the CMCs were performed by the BIH Proteomics Core Facility as previously described (Damerau et al., 2022). Protein extracts were digested with trypsin and peptides were analyzed by LC-MS/MS in data-dependent-mode on an Orbitrap Thermo instrument, followed by raw data analyses using MaxQuant software package. A minimum of three LFQ intensity values in at least one group was required. Missing values were imputed with low-intensity values simulating the detection limit of the mass spectrometer. Differences in protein abundance between the groups were calculated using the two-sample Student's t-test. Proteins passing the FDR-based significance cut-off of 5 %/10 % were considered differentially expressed.

2.8. RNA isolation, cDNA synthesis, and qPCR

RNA isolation using RNeasy® Fibrous Tissue Mini Kit (Qiagen GmbH, Germany), cDNA synthesis using TaqMan® Reverse Transcription Reagents Kit (Applied Biosystems Inc., USA), and quantitative PCR (qPCR) with the DyNAmo ColorFlash SYBR Green qPCR Kit (Thermo Fisher Scientific, USA) were performed as previously described (Damerau et al., 2020). The Stratagene Mx3000PTM (Agilent Technologies Inc., USA) was used for qPCR (duplicates per gene) with the following profile: 7 min at 95 °C, 60 cycles of 10 s at 95 °C, 7 s at 60 °C, and 9 s at 72 °C. Primer specificity (sequences listed in Table 3) was confirmed by product sequencing and melting curve analysis (data not

Table 3
Primer sequences.

Gene symbol	Gene name	Sequence of the forward primer	Sequence of the reverse primer
COL3A1	Collagen, type III, alpha 1	CTTTGTGCAAAAGGGGAGCT	TGGGTTGGGGCAGTCTAATT
CXCR4	C-X-C chemokine receptor type 4	GCATGACGGACAAGTACAGGCT	AAAGTACCAGTTTGCCACGGC
DCN	Decorin	CCTTTGGTGAAGTTGGAACG	TCGCACTTTGGTGATCTCAT
EF1A	Elongation factor 1 alpha 1	TGTGCTGTCCTGATTGTTGC	GTAGGGTGGCTCAGTGGAAT
FN1	Fibronectin 1	GGTGACACTTATGAGCGTCCTAAA	AACATGTAACCACCAGTCTCATGTG
FSP1	Fibroblast-specific protein 1	TCTTGGTTTGATCCTGACTGCT	TCACCCTCTTTGCCCGAGTA
GLUT1	Glucose transporter 1	AACCACTGCAACGGCTTAGA	TCACGGCTGGCACAAAACTA
HAS2	Hyaluronan synthase 2	TGTCGAGTTTACTTCCCGCC	CAGCGTCAAAAGCATGACCC
HIF1A	Hypoxia-inducible factor 1	CCATTAGAAAGCAGTTCCGC	TGGGTAGGAGATGGAGATGC
IL1B	Interleukin−1b	AGCTACGAATCTCCGACCAC	CGTTATCCCATGTGTCGAAGAA
IL6	Interleukin−6	AAGCAGCAAAGAGGCACTGG	TGGGTCAGGGGTGGTTATTG
IL8	Interleukin−8	CAGAGACAGCAGAGCACACA	TGGGGTGGAAAGGTTTGGAG
LDHA	Lactate dehydrogenase A	ACCCAGTTTCCACCATGATT	CCCAAAATGCAAGGAACACT
MMP1	Matrix metallopeptidase 1	CTCTGGAGTAATGTCACACCTCT	TGTTGGTCCACCTTTCATCTTC
MMP13	Matrix metallopeptidase 13	TCCTGATGTGGGTGAATACAATG	GCCATCGTGAAGTCTGGTAAAAT
MMP3	Matrix metallopeptidase 3	ATCCTACTGTTGCTGTGCGT	CATCACCTCCAGAGTGTCGG
PGK1	Phosphoglycerate Kinase 1	ATGGATGAGGTGGTGAAAGC	CAGTGCTCACATGGCTGACT
TNFA	Tumor necrosis factor-alpha	TCTGGGCAGGTCTACTTTGG	ATCCCAGGTTTCGAAGTGGT
VEGFA	Vascular endothelial growth factor A	AGCCTTGCCTTGCTGCTCTA	GTGCTGGCCTTGGTGAGG
VIM	Vimentin	GGACCAGCTAACCAACGACA	AAGGTCAAGACGTGCCAGAG

shown). Gene expression results were normalized to the housekeeping gene *EF1A*.

2.9. Generation of the synovial membrane model

The synovial membrane model was developed using the xeno-free VitroGel® RGD hydrogel (TheWell Bioscience Inc., North Brunswick Township, USA). To allow for sufficient nutrient supply, the model was cultured in a 24-well plate hanging insert with a pore size of 8 µm (Sarstedt, Hildesheim, Germany). Therefore, the polycarbonate membrane was coated with 100 µL hydrogel (1:3 gel-solution) containing 1×10^5 cells and polymerized for 30 min at RT. Synovial membrane models were cultivated for up to 21 days in a humidified atmosphere (37 °C, 5 % CO_2). The medium contains DMEM GlutaMAX™ supplemented with 2 % human AB serum (Capricorn Scientific, Ebsdorfergrund, Germany) and 1 % penicillin/streptomycin, in the following referred to as NM-XF.

2.10. Short- and long-term exposure to inflammatory stimuli

To mimic cytokine-mediated joint inflammation, stimulation was performed in NM-XF using 10 ng/mL rh macrophage migration inhibitory factor (MIF), 30 ng/mL rh interleukin (IL)-6, and 10 ng/mL rh tumor necrosis factor (TNF)-α (all ImmunoTools GmbH, Friesoythe; Germany), referred as +Cyt. The medium was changed every three days, including the respective supplements, resulting in a repetitive chronic cytokine stimulation. Incubation was conducted for 3 days (short-term) and 21 days (long-term) at 37 °C in a 5 % CO_2 atmosphere.

2.11. Cytotoxicity and viability assay

Cytotoxicity Detection LDH Kit (Sigma-Aldrich, Munich, Germany) was performed according to the manufacturer's instructions and as previously described (Damerau et al., 2020). Cell death was induced by 4 % (v/v) Triton™ X-100 (Sigma-Aldrich, Munich, Germany) for 24 h (high control). ApoTox-Glo™ Triplex Assay was performed according to the instructions of Promega Corporation (Walldorf, Germany) using phenol red-free DMEM (Gibco, Waltham, MA, USA). Cell death was induced by 4 % (v/v) Triton™ X-100 for 4 h or 100 µg/mL digitonin (Boehringer Mannheim GmbH, Mannheim, Germany) for 30 min, whereas apoptosis was induced by 0.1 mM camptothecin (Sigma-Aldrich) for 4 h.

2.12. BrdU proliferation assay

According to the manufacturer's instructions, the proliferation assay was performed using the BrdU (colorimetric) assay (Roche, Mannheim, Germany). The BrdU labeling solution was added to the cell culture medium on the synovial membrane model 20 h before endpoint measurement. Cells were fixed for 30 min at RT, followed by the addition of an anti-BrdU-POD working solution. After 90 min, cells were washed three times with 1x PBS, substrate solution was added, and incubation was stopped with 25 µL 2 N H_2SO_4 after 30 min. Measurement was performed at 450 nm (reference wavelength 630 nm). In addition, cells were treated with 1 µg/mL actinomycin D (Sigma-Aldrich, Munich, Germany) to suppress proliferation (negative control).

2.13. Glucose and lactate concentration

Glucose and lactate content – as a measure of glycolysis – were analyzed using the Biosen C-Line Glucose and Lactate analyzer (EKF-diagnostic GmbH, Barleben, Germany). For this, 20 µL supernatant was mixed with 1 mL PBS, while instrument calibration and electrode validation were performed with the manufacturer's solutions before the measurements.

2.14. Statistics

Statistical analyses were performed using the software GraphPad® Prism Version 9.3.0 (La Jolla, San Diego, CA, USA). Since the data sets were not normally distributed, non-parametric tests were performed. Mann-Whitney U test was used for direct comparisons of two independent datasets. For comparisons of more than two independent datasets, one-way analysis using Kruskal-Wallis with Dunn's multiple comparisons test was performed. A two-tailed Wilcoxon matched-pairs signed-rank test was applied for dependent datasets. For comparisons of more than two dependent datasets, one-way analysis using Friedman with Dunn's multiple comparisons test was performed. P-values of <0.05 were considered statistically significant (*p <0.05, **p <0.01, ***p <0.005). Data are shown as box plots (centerline, median; box limits, upper and lower quartiles; whiskers, maximum and minimum) if not indicated otherwise.

3. Results

3.1. Comparative phenotypic analysis of human knee-derived FLSs from trauma patients and bone marrow-derived MSCs

Hypothesizing that non-inflamed FLSs own similar features to MSCs, we compared the phenotypic attributes of FLSs isolated from patients with ligament injuries (trauma-FLSs) with those of MSCs in a comprehensive manner. Therefore, we firstly analyzed the isolated cells during their second passage using standardized protocols for the characterization of MSCs based on the minimal criteria to define human MSCs as proposed by the Mesenchymal and Tissue Stem Cell Committee of the International Society for Cellular Therapy (Damerau et al., 2022, 2020). We observed for both cell types the adhesion to plastic surfaces and the characteristic spindle-shaped morphology of mesenchymal cells as visualized by brightfield microscopy (Fig. 1A). Both cell types could be successfully differentiated into an adipogenic or osteogenic lineage after 21 days, as evidenced by the formation of lipid droplets positive for Oil-Red-O and mineralization positive for Alizarin Red staining, respectively (Fig. 1A), emphasizing their mesenchymal character. Flow cytometric analysis of MSCs and FLSs showed similar expression patterns for stem cell markers such as CD105, CD73, and CD90, whereas negative markers such as CD14, CD20, CD34, CD45, and HLA-DR were almost absent (Fig. 1B).

This similarity in surface marker profiles suggests a close phenotypic relationship between FLSs and MSCs. Due to their heterogeneity and lack of a specific marker, identifying FLSs and MSCs remains challenging. Traditionally, FLSs have been determined using the mesenchymal marker vimentin. However, recent studies have shown that subgroups of FLSs in RA differ in their expression of thymic cell antigen 1 (THY1, CD90). In contrast, podoplanin (PDPN) expression is associated with severe chronic inflammation (Astarita et al., 2012; Damerau et al., 2022; Mizoguchi et al., 2018). In our study, visualization of THY1^{+} cells confirmed the flow cytometry results and showed a similar expression pattern of PDPN in both MSCs and FLSs (Fig. 1C). The comparable expression of PDPN in both cell types suggests a

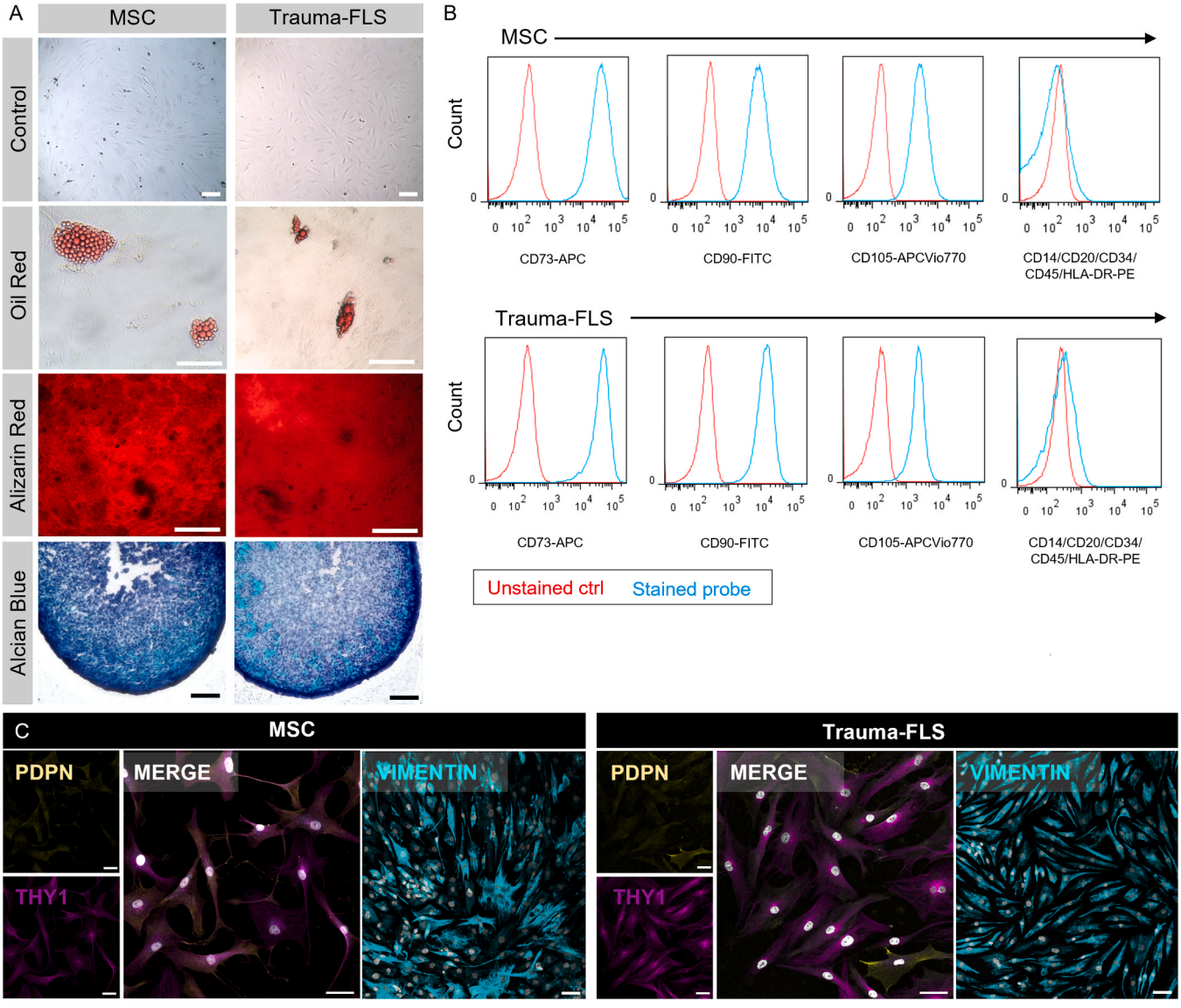

Fig. 1. Phenotypic characterization of trauma-FLSs compared with bone marrow-derived MSCs. (A) MSCs and FLSs adhere to plastic and show spindle-shaped cell morphology. Representative images of the Oil Red (adipogenesis), Alizarin Red S (osteogenesis), and Alcian Blue (chondrogenesis) staining demonstrate their ability to differentiate into multiple lineages. Scale bars show 100 μm. (B) Flow cytometry was used to investigate the expression of CD73, CD90, and CD105 and the absence of CD14, CD20, CD34, CD45, and HLA-DR. (C) Exemplary images comparing MSCs and trauma-FLS regarding THY1(magenta), PDPN (yellow), vimentin (cyan), and DAPI (gray). Scale bars show 50 μm.

non-inflammatory phenotype of MSCs, further supporting the potential of MSCs as a valuable cell source for engineering "healthy" tissue.

Furthermore, to elucidate the metabolic differences between MSCs and trauma-FLSs, we utilized Seahorse™ technology, which is a rapid and robust methodology to measure mitochondrial oxygen consumption rate (OCR) and extracellular acidification rate (ECAR) of living cells (Fig. 2). We first performed the Mito Stress Test assay, in which OCR is assessed at baseline and then following stepwise application of mitochondrial inhibitors via the instrument ports. Our results show that trauma-FLSs exhibit decreased basal respiration and mitochondrial ATP production compared to MSCs (Fig. 2A), which is consistent with an observed slightly higher ECAR (Fig. 2B, C). In addition, trauma-FLSs showed a significantly higher spare capacity (Fig. 2D), indicating more mitochondria in FLSs. This observation is consistent with a previous study on FLSs derived from patients with OA (Damerau et al., 2022). The slight increase in proton efflux rate (PER) observed in trauma-FLSs aligns with the ECAR profile. This suggests that MSCs favor oxidative phosphorylation (OXPHOS) over trauma-FLSs for energy production.

3.2. Impact of CTGF, IGF, and FGF on MSC differentiation into FLS-like cells

In a second approach, we examined the potential of CTGF (100 ng/mL) and its combination with either FGF (10 ng/mL) or IGF (10 ng/mL) as well as both together to differentiate bone marrow-derived MSCs into FLSs. Previous studies have focused on proteins of the ECM such as collagens and the cytoskeleton such as vimentin as evidence of differentiation (Lee et al., 2006, 2010b; Xu et al., 2015). Here, we examined a broader range of fibroblast markers to understand this differentiation pathway better. MSCs were stimulated and cultured for three weeks in comparison to an untreated control. Using real-time PCR, we analyzed the expression of various fibroblast markers, including fibronectin (*FN1*), collagen III (*COL3A1*), fibroblast-specific protein (*FSP1*), decorin (*DCN*) and hyaluronan synthase 2 (*HAS2*) after 7, 14 and 21 days of incubation. We demonstrate an increase in all fibroblast markers in all conditions tested after 21 days in combination (Fig. 3). After 7 days of stimulation, in particular, *FN1* gene expression of the major component of the extracellular matrix was significantly higher in the CTGF+IGF group compared to the control group. The expression of *DCN* , a key protein of the ECM involved in cell signaling, was also significantly higher in the CTGF group than in the control group. In addition, we observed a significant increase in *COL3A1* expression in MSCs treated with CTGF+FGF after 7 days.

After 14-day stimulation, *FN1* gene expression decreased in all treatment groups but was still higher in the CTGF group than in the control group, indicating an early response to CTGF stimulation. Also, *COL3A1* expression significantly increased after treatment with CTGF+IGF. After 21 days, *FN1* gene expression increased compared to the values observed after 14 days. Moreover, *COL3A1* expression significantly increased after treatment with CTGF alone. Gene expression of *HAS2*, an enzyme crucial for synthesizing hyaluronan, a major component of synovial fluid was significantly enhanced after 21 days of stimulation with CTGF compared to unstimulated MSCs. However, it is important to note that no significant differences were observed in the expression of *VIM* , *FSP1,* and *PDPN*, indicating the selective effects of CTGF on the expression of fibroblast markers.

To assess the viability of MSCs after 21 days of the different treatments, Live-Dead staining was applied and showed that the stimulation did not affect cell survival (Fig. 4). In addition, we observed that stimulated cells showed a spindle-shaped morphology and a higher cell confluence than untreated MSCs – a morphology characteristic for fibroblast differentiation.

To confirm gene expression data, we examined the protein expression of HAS2 and VIM. Remarkably, HAS2 expression was most pronounced in cells treated with CTGF (Fig. 4). In contrast, the stability of VIM staining was not affected regardless of treatment, suggesting selective effects of stimulation on fibroblast-specific protein expression and confirming the result from the gene expression analyses (Fig. 4). In summary, our results show that CTGF especially effectively induces MSC activation. The selective expression of certain fibroblast markers and the stability of others, such as vimentin, emphasize the complexity of MSC differentiation and the different roles of various growth factors in this process.

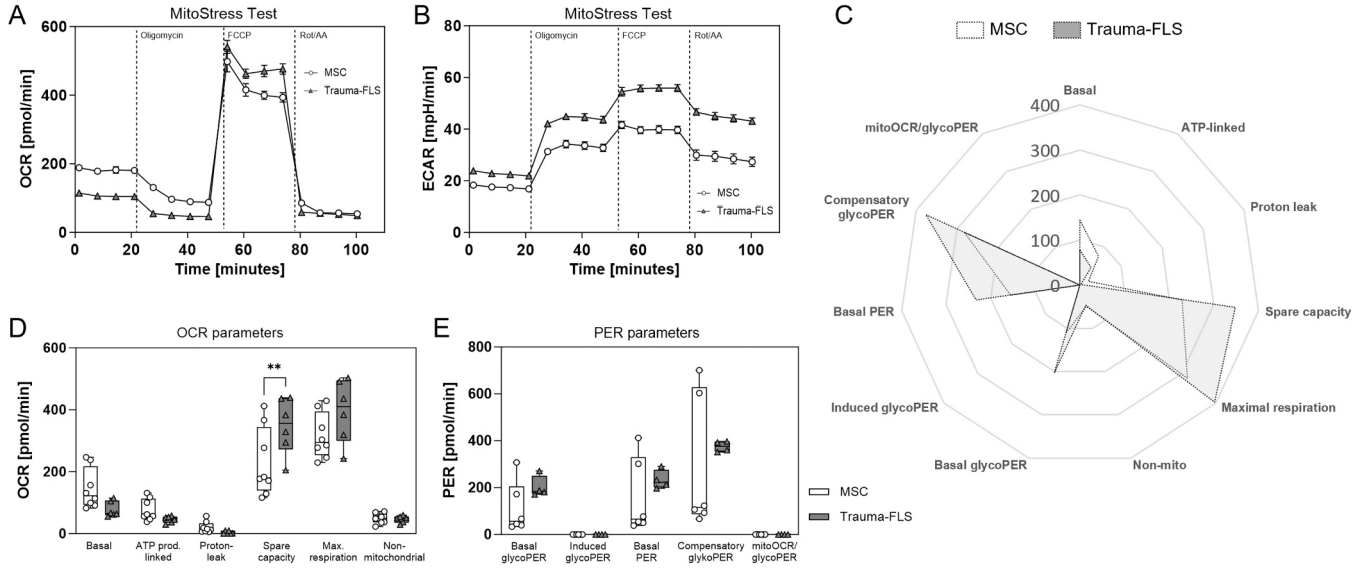

Fig. 2. Metabolic profile of MSCs and trauma-FLSs. (A) Seahorse XF Mito Stress Test data for oxygen consumption rate (OCR) and (B) extracellular acidification rate (ECAR) were assessed over time, before or after addition of 2 μM oligomycin 1.5 μM FCCP, and 0.5 μM Rot/AA. Data represent 5 technical replicates. (C) Radar plot summarizing the values obtained for each parameter of the Seahorse XF Mito Stress Test and Glycolytic Rate Assay as a fraction of the average of all measures obtained for the same parameter. (D) Results of the Mito Stress Test (n=6–8) and (E) Glycolytic Rate Assay (n=4–6) are shown in pmol/min/10^5 and represent 5 technical replicates. Data are shown as box plots (centerline, median; box limits, upper and lower quartiles; whiskers, maximum and minimum values; all data points). Statistical analysis was performed using a mixed-effects model with the Geisser-Greenhouse correction and Šídák's multiple comparisons test. The resulting p-values are indicated in the figures with **p <0.01.

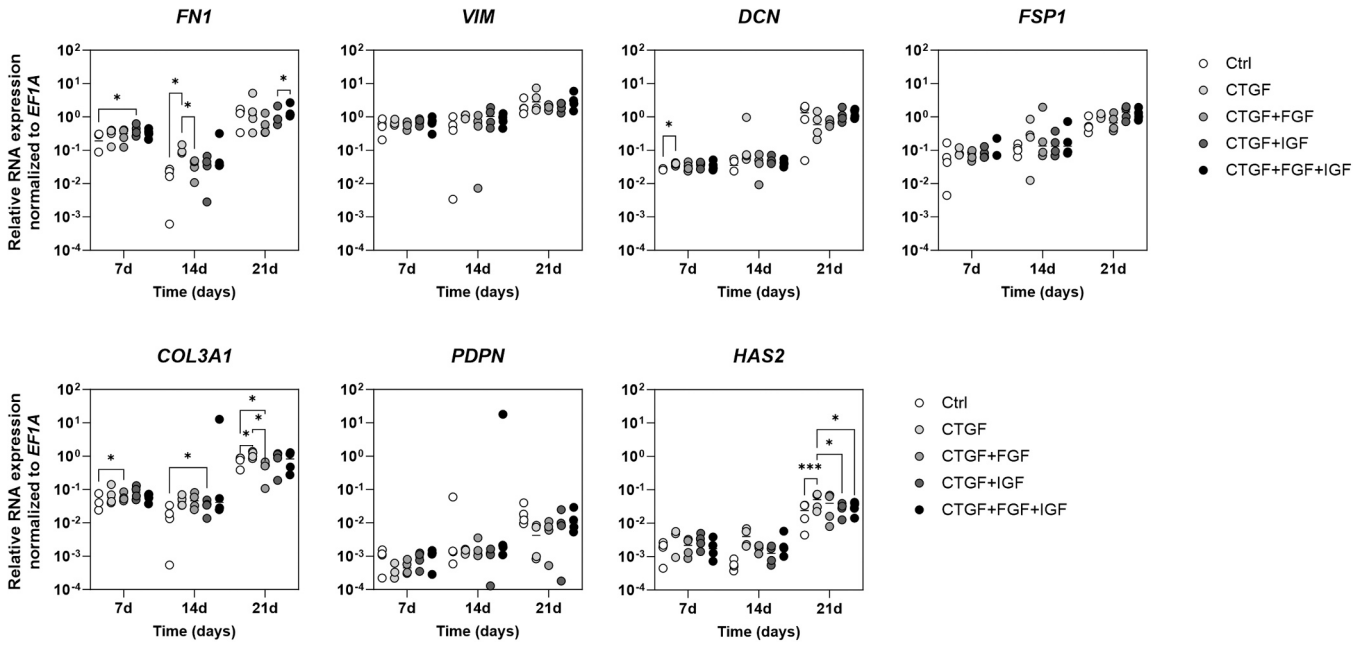

Fig. 3. CTGF stimulation exerts distinct effects on fibroblastic differentiation of MSC on mRNA level. Fibroblast-specific markers were progressively increased after 7, 14, and 21 days of treatment. Data are represented as scatter dot plots with the median. Statistical analysis was performed using a mixed-effects model with the Geisser-Greenhouse correction and Tukey's multiple comparison test, with individual variances calculated for each comparison. The resulting p-values are indicated in the figures with *p <0.05, ***p <0.001.

3.3. Global and unbiased identification of the differentially expressed proteins in OA-FLS, MSCs, and CTGF-differentiated MSCs

To identify proteins altered in MSCs by CTGF treatment on a global level, especially in comparison to OA-FLS, we performed proteome analysis using liquid chromatography-tandem mass spectrometry (LC-MS/MS). First, we performed principal component analysis (PCA) to compare MSC, and OA-FLS, with NHDF cells (normal human dermal fibroblasts) commonly used in *in vitro* 3D modeling. PCA showed that fibroblast types clustered according to their origin (Fig. 5A). Interestingly, synovial fibroblasts and bone marrow-derived MSCs were more closely related on proteome level (Fig. 5A). With regard to CTGF treatment, our analysis identified 57 differentially expressed proteins between the CTGF-treated MSCs and the control group using a two-sample (paired) t-test with a false discovery rate (FDR) cut-off of 5 % (Fig. 5B). Focusing on classical MSC and fibroblast markers, we identified collagens to be highly expressed in both the MSC and CTGF-treated groups (Fig. 5C, D). In contrast, aminopeptidase E (ANPEP), previously detected in OA synovial fluid (Balakrishnan et al., 2014), and MMP2 were higher expressed in OA-FLS (Fig. 5C, D). Interestingly, hyaluronan-related proteins showed no significant differences between all groups, including CTGF treatment (Fig. 5E). An important observation of our study is that proteome profiles of MSCs and CTGF-treated MSCs do not completely correlated despite sharing common features. This includes different expression patterns of known marker genes and highlights the complexity of MSC differentiation under the influence of CTGF. In summary, our proteomic analysis provides valuable insights into the effects of CTGF on MSCs, particularly on OA-FLS. The differential expression of key proteins such as collagens, ANPEP, and MMP2 highlights the distinct proteomic signatures of these cell types and the differential effects of CTGF on MSCs.

Analyzing similarities between MSCs stimulated with CTGF and the protein expression profile of OA-FLS, we observed that proteins such as serpin family B member 2 (SERPINB2), lysyl oxidase-like 4 (LOXL4), latent transforming growth factor beta binding protein 1 (LTBP1), sulfite oxidase (SUOX), integrin subunit beta 3 (ITGB3), and intercellular adhesion molecule 1 (ICAM1) were upregulated in CTGF-treated MSCs, similar to OA-FLS (Fig. 6A). In addition, certain proteins, including integrin subunit beta 1 (ITGB1) and collagen type 1, were less expressed in CTGF-treated MSCs and OA-FLS. Conversely, proteins such as podocan (PODN), SERPINB2, oligoadenylate synthetase (OAS), and interferon-induced GTP-binding protein MX1 were most highly expressed in the CTGF group. Interestingly, the expression of fibroblast markers (e.g., VIM, TNC, DCN, FSP1, and FN1) and MSC markers (e.g., THY1, ecto-5′-nucleotidase (NT5E; CD73) and endoglin (ENG)) remained unaffected by CTGF stimulation (Fig. 6B, C). However, FSP1 was significantly higher in OA-FLS, while FN1 was substantially lower expressed. Regarding cell metabolism, our data showed that CTGF-treated MSCs had considerably higher levels of carnitine palmitoyltransferase 1 A (CPT1A), indicating a shift in metabolism towards increased fatty acid oxidation (Fig. 6D). This result is particularly interesting as it implies a possible metabolic adaptation of MSCs under CTGF influence. In addition, our comparative analysis of proteins involved in fibrosis showed that MSCs express more proteins associated with fibrosis than OA-FLS, which was further enhanced by CTGF treatment, increasing the expression of markers such as smooth muscle actin alpha (ACTA), LTBP1, and SEPINE1 (Fig. 6E). Functional comparison of trauma-FLSs and MSCs in terms of cell proliferation, demonstrated a lower proliferation rate in FLSs than MSCs (Fig. 6F). In contrast, both, CTGF-stimulated MSCs and OA-FLSs showed a significantly higher proliferation. Our investigation of the classical fibroblast marker genes showed similar expression profiles at both protein and mRNA levels. CTGF treatment significantly enhanced *HAS2* gene expression (Fig. 6G). Of note, *FN1* was downregulated in OA-FLS at both protein and RNA levels, correlating with disease status (Fig. 6G).

In summary, our results demonstrate no significant differences between MSCs and trauma-FLSs. However, treatment of MSCs with CTGF results in changes in ECM protein expression and a higher proliferation rate that bring them more in line with OA-FLSs and point to a potential role of CTGF in modulating the behavior and properties of MSCs towards an activated fibroblast-like phenotype.

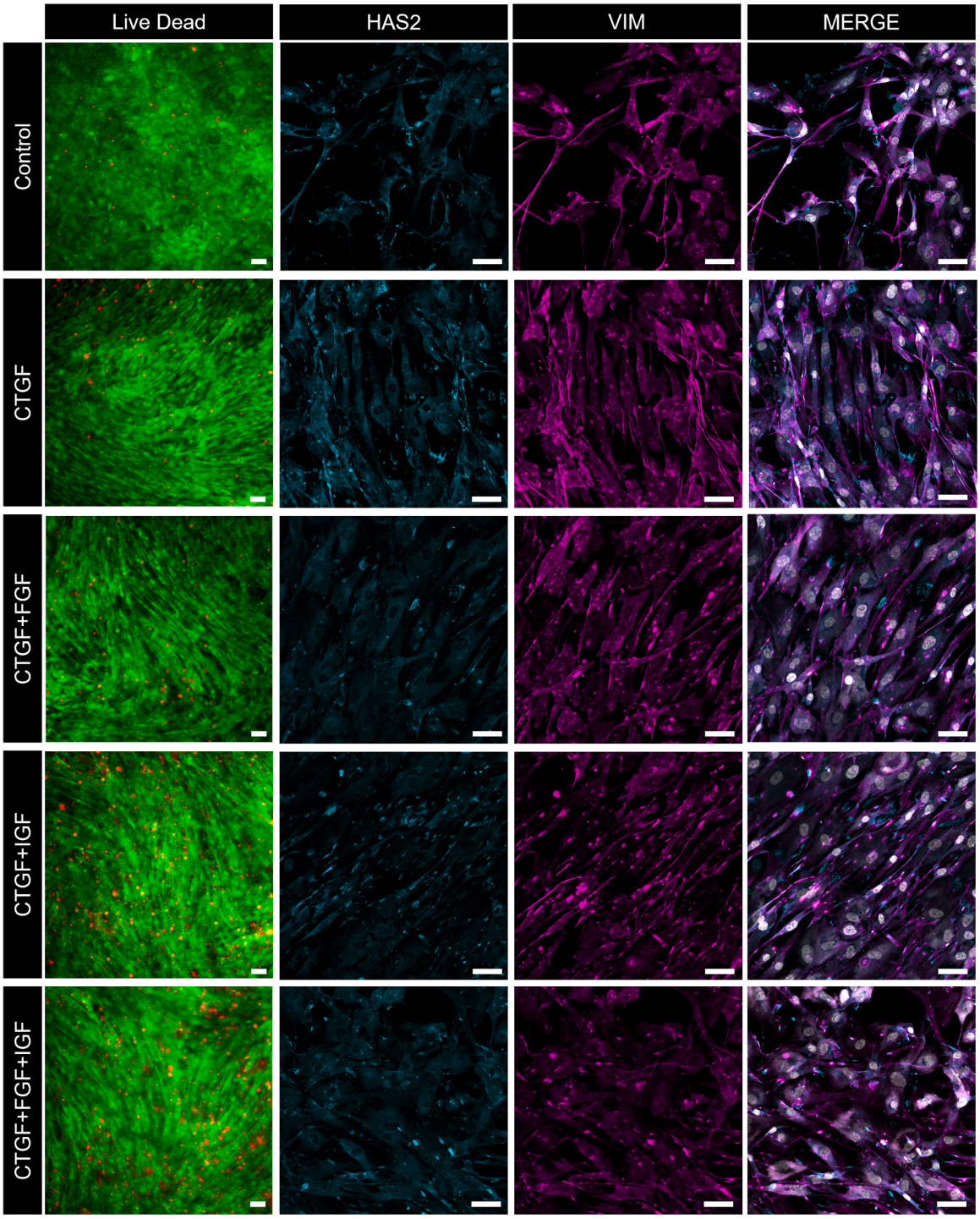

Fig. 4. Cell morphology is affected by long-term exposure of MSCs to CTGF. Exemplary image for the untreated control group of mesenchymal stromal cells, cells treated with CTGF alone and combined with FGF and IGF. Live Dead, HAS2 (cyan), vimentin (magenta), and DAPI (gray). The scale bar shows 100 μm.

3.4. Mimicking the geometry of the synovial membrane using a biocompatible 3D hydrogel construct

As demonstrated in the previous sections of our study, the application of CTGF tends to shift MSCs towards a more activated state, which may not accurately reflect the conditions of non-diseased joint tissues. To develop an *in vitro* model that more closely represents the healthy, non-activated state of joint tissues, we created a 3D synovial lining layer using untreated MSCs representative of the synovial membrane in its natural, non-pathological state. Therefore, we have imitated the following three features of the synovial lining layer:

- The synovial membrane is characterized by its lack of a basement membrane and tight junctions (Kiener et al., 2006).
- It is a loose composite of cells embedded in an amorphous matrix composed of collagens such as collagen type I and III (Kiener et al., 2006; Orr et al., 2017).
- The intimal lining is typically one to four cell layers thick and directly contacts the synovial fluid within the joint cavity.

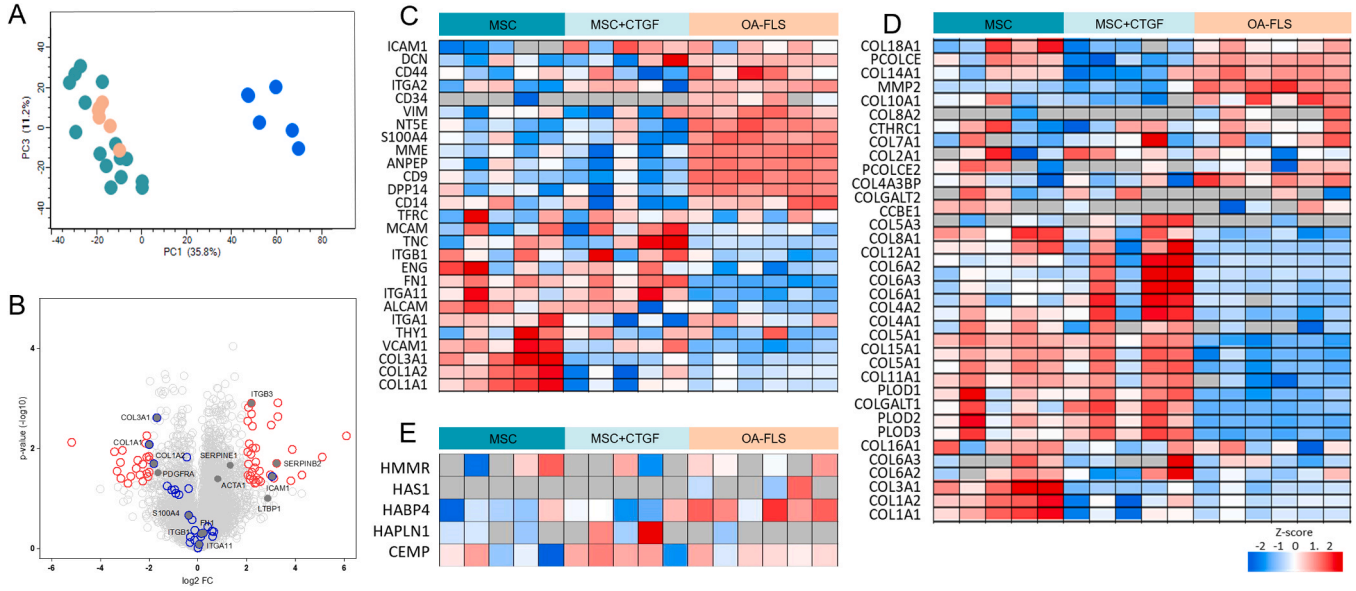

Fig. 5. Distinct protein expression between CTGF-treated MSC, untreated MSCs, and OA-FLS. (A) PCA analysis comparing MSCs (green, triplicates for n=5), OA-FLS (orange, n=5), and NHDF (blue, n=6) cells. (B) Volcano plot of proteome data (LFQ intensities) comparing CTGF-treated MSCs and untreated MSCs. We identified 57 significant differentially expressed proteins. The colored dots indicate significant differentially expressed proteins (red; false discovery rate (FDR) of 5 % cut-off) and selected cell-specific marker genes (blue). (C) Heatmap with non-imputed data showing MSC and FLS-related markers, (D) collagen-specific markers, and (E) hyaluronan-specific markers. The grey color indicates a missing value; NA = not detected, under the detection limit (n=5).

To replicate this environment, we used synthetic hydrogel to embed cells, creating a simplified 3D model of the synovial lining membrane. The model was cultured on a polycarbonate-based hanging insert, allowing for apical and basal nutrient supply. Our initial experiments established that embedding $1*10^5$ cells within the hydrogel yielded an optimal confluent layer of viable cells. To assess the biocompatibility of our hydrogel, we conducted an LDH assay. The results demonstrated no significant LDH release in the hydrogel samples compared to the high control, indicating that the hydrogel did not induce cytotoxicity (Fig. 7A). Further analysis of cell viability, cytotoxicity, and programmed cell death (apoptosis) after 21 days of incubation within the synthetic hydrogel revealed a predominance of viable, non-cytotoxic, and non-apoptotic cells (Fig. 7B). LIVE/DEAD staining showed a confluent layer of viable Calcein AM-positive cells (Fig. 7C, D). To assess the distribution and density of cells within the hydrogel, tissue sections were stained for F-actin and examined horizontally and vertically. The horizontal analysis confirmed a uniform distribution of cells, with two to three cell layers evident on the z-axis. This observation was corroborated by the vertical section analysis, which also supported a multi-layered cell structure within the hydrogel (Fig. 7E, F). Our data demonstrate that the simplified model fulfilled the synovial layer's three characteristics.

3.5. Short-term exposure to inflammatory stimuli leads to an inflammatory gene expression, while long-term exposure results in hyperproliferation of the synovial membrane model

To validate the functional responsiveness of our animal-free synovial membrane model, we exposed it to a pro-inflammatory cytokine cocktail comprising TNF-α, IL-6, and macrophage migration inhibitory factor (MIF). These cytokines induce hypoxia-adaptive responses, angiogenesis, and invasiveness within the synovial membrane. The concentrations used were previously established as non-cytotoxic (Damerau et al., 2020). The model was stimulated for two distinct periods: 3 days and 21 days, and the results were compared with those from an untreated control group. After short-term exposure (3 days), we observed significant increases in cellular proliferation and glucose uptake, key markers of glycolytic activity (Fig. 8A, B). Additionally, the cytokine-treated cells exhibited increased thickness and enhanced expression of PDPN, an indicator of cellular activation (Fig. 8C). Regarding gene expression, the cytokine stimulation markedly upregulated pro-inflammatory markers, significantly increasing *IL6* and *IL8* expression. *TNFA* also tended to have higher expression following short-term exposure than the untreated control (Fig. 8D). Furthermore, the pro-inflammatory environment substantially increased the expression of vascular endothelial growth factor A (*VEGFA*) and phosphoglycerate kinase 1 (*PGK1*), which are key mediators in angiogenesis and glycolytic processes, respectively. *LDHA* expression also tended to increase under these conditions. However, the expression levels of glucose transporter 1 (*GLUT1*) remained similar to those in the untreated control group (Fig. 8E).

We further explored the inflammatory response of the animal-free synovial membrane model using repetitive long-term exposure to better mimic the chronic aspects of inflammatory joint diseases such as rheumatoid arthritis. A key characteristic of arthritis is synovial hyperplasia, so we focused on the proliferation rate in the lining layer of the synovial membrane. After comparing results from short-term (3 days) and long-term (21 days) exposure, we found a marked increase in lining layer proliferation following the 21-day exposure period (Fig. 9A). After long-term exposure, a significant increase in *IL8* expression was observed on the gene expression level. However, other pro-inflammatory markers, such as *TNFA*, *IL6*, and *IL1B*, only increased numerically but not significantly (Fig. 9B). This suggests a nuanced and specific inflammatory response over time. Given the distinctive invasiveness of fibroblasts during inflammation, we also analyzed the expression of MMPs, which play a crucial role in tissue remodeling and inflammation. Notably, long-term exposure to the inflammatory cytokines significantly increased the expression of *MMP1* and *MMP13* compared to the untreated control (Fig. 9C). This indicates enhanced tissue-remodeling capabilities under chronic inflammatory conditions. Another hallmark of inflammation is hypoxia, often marked by the interplay between MIF and hypoxia-inducible factor (HIF)-1. In our model, we observed a significant upregulation of HIF-1 under long-term exposure (Fig. 9D), underscoring the model's ability to replicate key features of the inflammatory environment in synovial membranes.

In conclusion, our study has successfully established a simplified human-based *in vitro* model of the synovial membrane using a synthetic

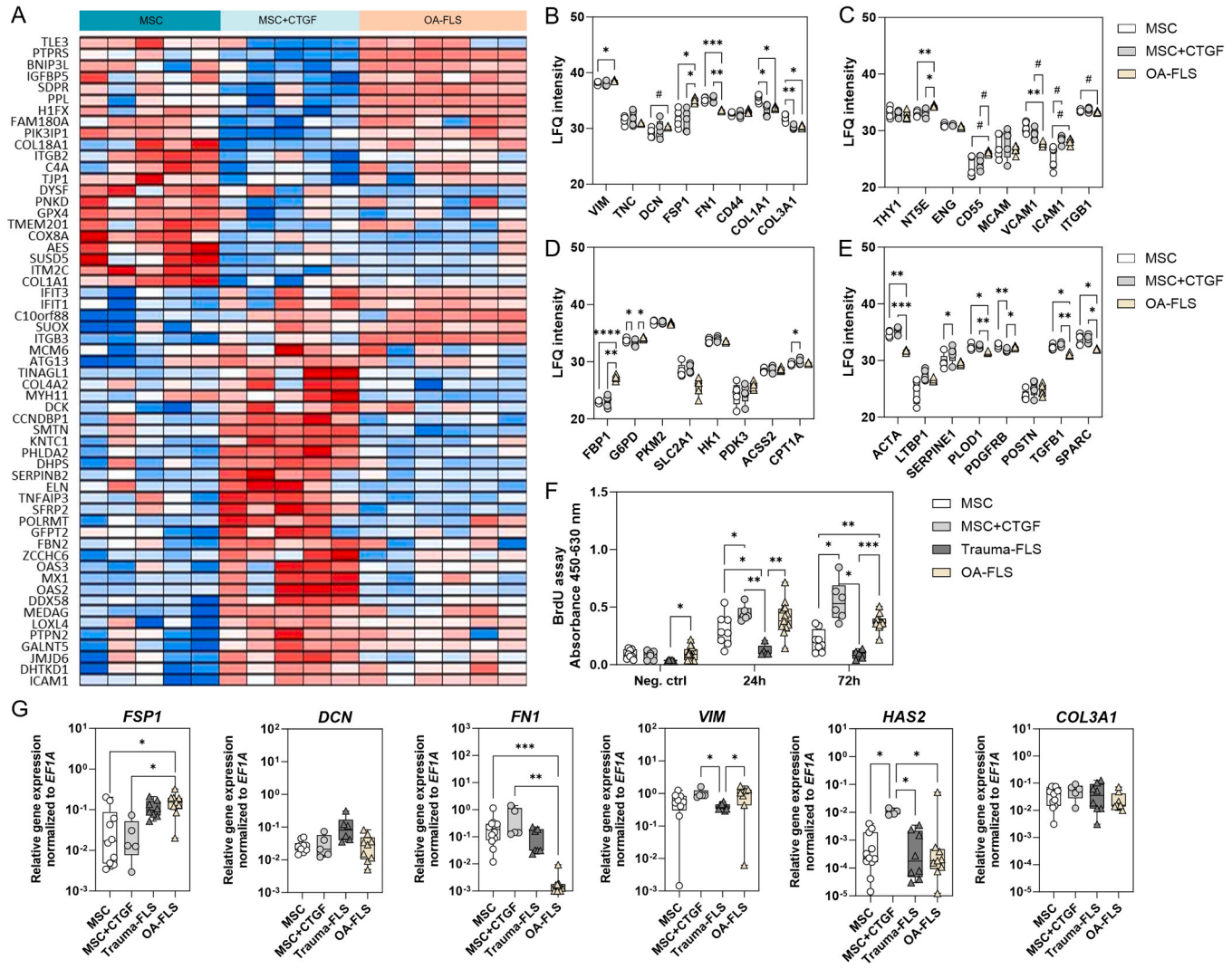

Fig. 6. CTGF induces a proliferative, profibrotic phenotype. (A) Heatmap with all samples of the 57 significant proteins determined using a two-sample (paired) t-test with a false discovery rate (FDR) of 5 % cut-off. (B) Protein abundance of classical fibroblast markers, (C) MSC-related markers, (D) metabolic markers, and (E) fibrotic markers (n=5–6). Shown are log2 transformed LFQ intensity values. (F) BrdU assay was conducted after 24 h and 72 h to explore the proliferation rate (n=5–13). Cells were treated with 1 μg/mL actinomycin D (neg. ctrl) to suppress the proliferation. (G) Total RNA extraction was performed from undifferentiated MSCs and after differentiation with 100 ng/mL CTGF for three weeks compared with FLS from trauma and OA patients (n=5–10). Gene expression of classical fibroblast markers was performed using SYBR Green and normalized to the housekeeper gene *EF1A*. Data are shown as box plots (centerline, median; box limits, upper and lower quartiles; whiskers, maximum and minimum values). Statistical analysis for (B)-(F) was performed using a mixed-effects model with the Geisser-Greenhouse correction and Tukey's multiple comparison tests, with individual variances calculated for each comparison. Kruskal-Wallis with Dunn's multiple comparisons tests was performed in (G). P-values are indicated in the graphs with *p <0.05, **p <0.01, ***p <0.001.

hydrogel. Furthermore, the model's ability to dynamically respond to pro-inflammatory stimuli, reflecting key cellular and molecular changes seen in inflammatory joint diseases, validates its applicability for studying disease mechanisms and testing potential therapeutic interventions. Overall, these findings underscore the model's potential to provide insights into the pathophysiology of conditions of arthritis and to aid the development of novel treatment approaches.

4. Discussion

The potential of bone marrow-derived MSCs to differentiate into various cells, in conjunction with the presumed mesenchymal origin of synovial fibroblasts, has raised interest in exploring the differentiation capabilities of MSCs into fibroblastic cells. This investigation is particularly relevant for the purpose of tissue engineering and regenerative medicine. A novel aspect of our study is that we compared synovial fibroblasts from trauma patients with MSCs and investigated the CTGF-mediated fibroblastic transition of MSCs compared to OA-FLS. Moreover, we innovatively developed and characterized an animal-free, MSC-embedded, multilayered, RGD-functionalized hydrogel-based synovial construct. This construct mimics the morphology, functionality, and reactivity to inflammatory stimuli observed in native synovial tissue. Understanding the cellular mechanisms and interactions within the synovial membrane is important for developing and screening effective therapeutic strategies. This underscores the importance of robust *in vitro* models that can accurately replicate the complexity of the synovial environment. Within the study, we unrevealed that (i) human knee-derived FLS from trauma patients exhibit a stem cell-like phenotype similar to that of human bone marrow-derived MSCs, and (ii) CTGF induced the differentiation of MSCs toward the fibrotic fibroblast phenotype, both underlining the profound suitability of MSCs in the development of both healthy and diseased *in vitro* synovial constructs. Furthermore, our study also demonstrated (iii) the ability to mimic the geometry of the synovial membrane using a biocompatible, synthetic

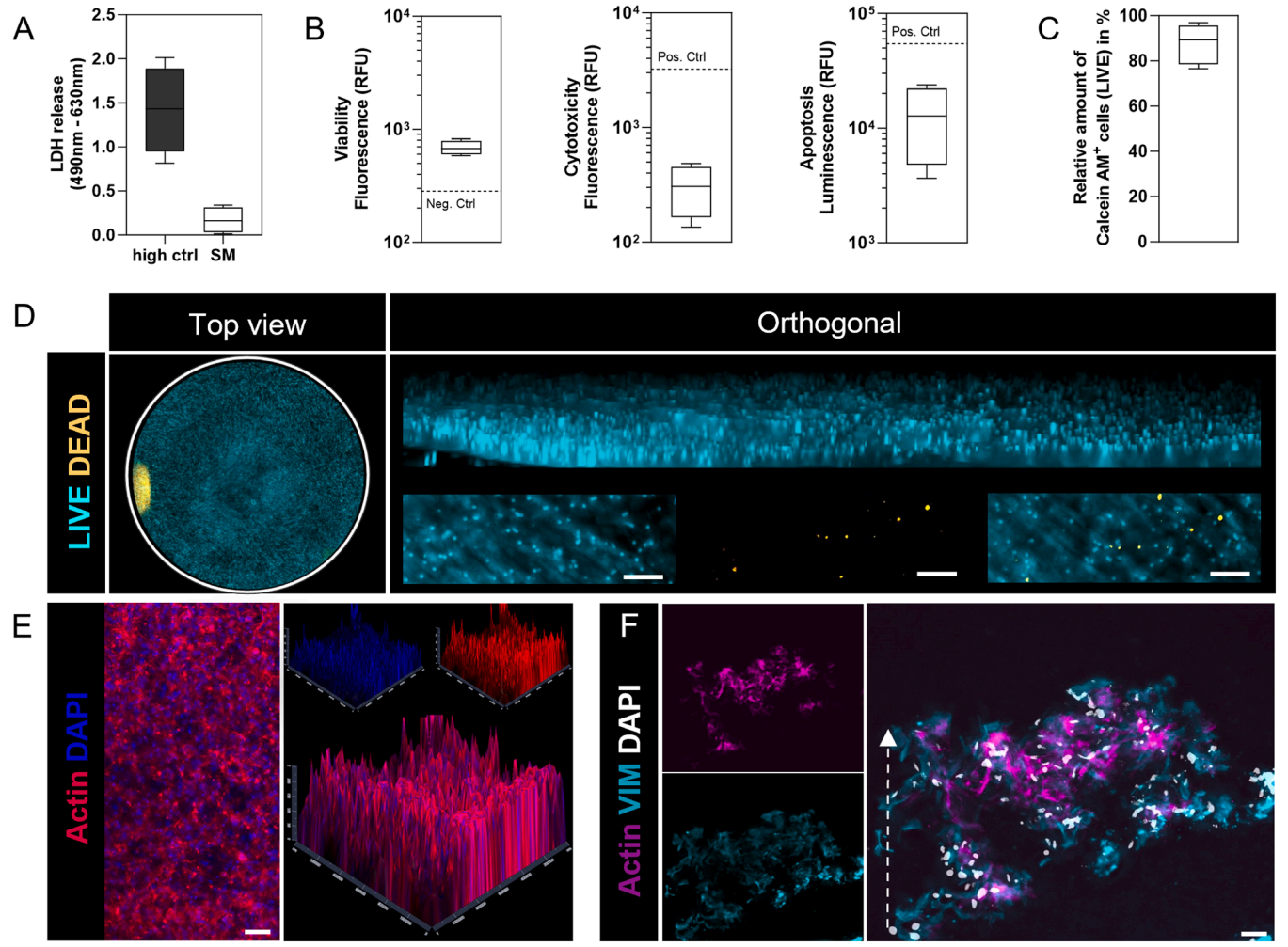

Fig. 7. The RGD-based synovial membrane results in a biocompatible 3D construct with a homogenous one to four cell layers thick lining. (A) LDH cytotoxicity assay was conducted after 24 h to confirm the biocompatibility of the synthetic hydrogel. High ctrl = 4 % Triton™ X-100 for 24 h; SM = synovial membrane model (n=4). (B) ApoTox-Glo™ Assay analyzing cell viability, cytotoxicity, and apoptosis level for n=4. Neg. Ctrl for viability: 100 µg/mL Digitonin. Pos. Ctrl for cytotoxicity: 4 % Triton™ X-100. Pos. Ctrl for apoptosis: 0.1 mM Camptothecin. (C) Relative number of viable cells was visualized using LIVE/DEAD staining. The staining was performed after 21 days and quantified using ImageJ (n=8). (D) Exemplary image of LIVE/DEAD staining. Living cells are presented in cyan (Calcein-AM+), and dead cells in yellow (EthD+). (E) Horizontal analysis of the synovial membrane. F-actin (red), DAPI (blue). (F) Vertical histological section. F-actin (magenta), vimentin (cyan), DAPI (grey). Scale bars = 100 µm. Statistics: Two-tailed Wilcoxon matched-pairs signed-rank test and Wilcoxon signed-rank test to the ctrl.

RGD-hydrogel supporting cell arrangement in a lining layer-like structure. In addition, (iv) exposure to inflammatory stimuli increased gene expression of pro-inflammatory, pro-angiogenic, and matrix-degrading proteins, increased proliferation, and a rise in glucose consumption, mirroring responses observed in human arthritis.

Fibroblasts occur in different tissues across the body. They are remarkably diverse between the various tissues and even within the same tissue, as different subsets of fibroblasts exist (Damerau et al., 2024). These have different functions. Recent research revealed, e.g., for synovial fibroblasts, that certain subtypes can be assigned to RA and others to OA (Damerau et al., 2024). Our previous research has shown that even after prolonged culture, OA-FLSs retain a disease-specific imprint characterized by the release of pro-inflammatory cytokines, high proliferation rates, and altered metabolism (Damerau et al., 2022). OA is characterized by chronic inflammation, which significantly impacts the behavior of resident cells.

However, similarities between OA-FLS and MSCs can be attributed to their biological functions, developmental origins, and responses to microenvironmental conditions, which can result in the expression of similar genes and proteins. There is general agreement that synovial fibroblasts originate from synovial tissue and are of mesenchymal origin. Their shared lineage might contribute to the expression of similar surface markers, transcription factors, and signaling molecules. However, there are two different views on the origin of synovium-derived MSCs. One view is that MSCs are brought to the synovium via migrating blood vessels. On the other hand, there is evidence that synovium-derived MSCs originate from the synovial intima (Matsuo et al., 2018). As our group has previously shown, OA-FLS and MSCs share common phenotypic features and are indistinguishable in terms of (i) morphology, represented as spindle shape, (ii) plastic adherence, (iii) multipotency potential, (iv) expression of mesenchymal cell surface markers, and (v) absence of hematopoietic cell surface markers (Damerau et al., 2022). This was also observed when comparing fibroblast strains from different tissue sources (Brohem et al., 2013a; Denu et al., 2016b; Lorenz et al., 2008a). In general, both MSCs and synovial fibroblasts are identified by a combination of nonspecific markers rather than by a specific marker. Although fibroblasts are assumed to be of mesenchymal origin, we first confirmed the stem cell-like phenotype of synovial tissue-derived trauma-FLSs compared to bone marrow-derived MSCs. The former is the most suitable inflammatory-unexposed control, as healthy patient-derived FLSs are not justifiable for ethical reasons.

Here, we show for the first time that trauma-FLSs and MSCs are also

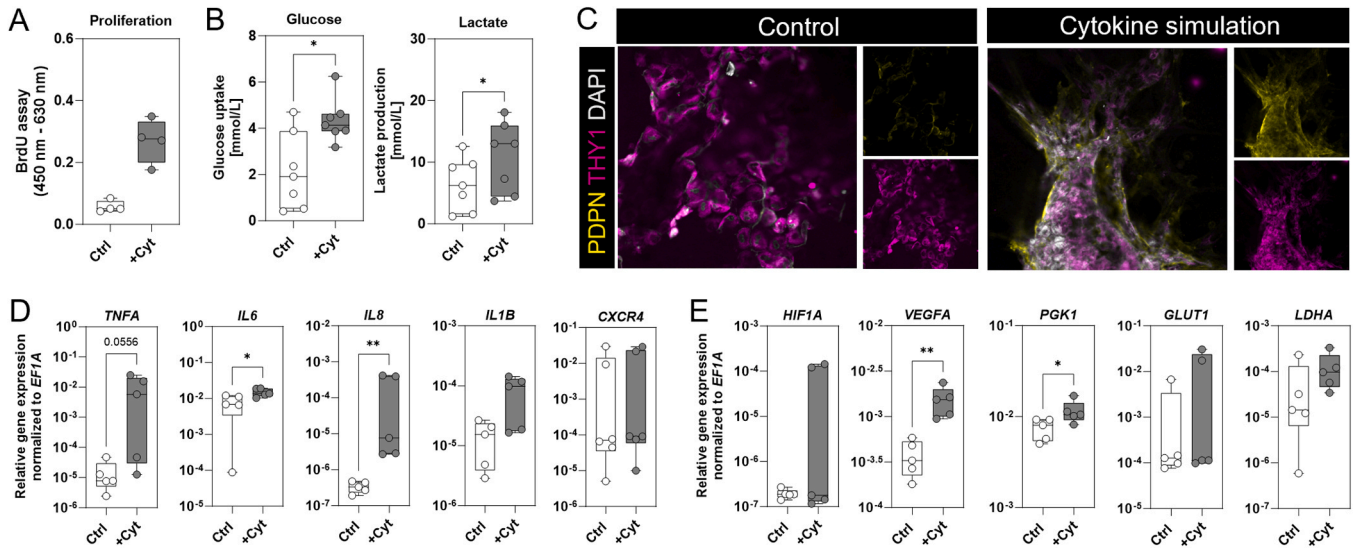

Fig. 8. Short-term exposure to inflammatory stimuli leads to enhanced glycolysis and induced gene expression of pro-inflammatory markers. (A) BrdU assay was conducted to explore the proliferation rate (n=4). (B) Glucose uptake and lactate production were analyzed after day 3 days (n=7). (C) Exemplary top-view images comparing short-term exposure with the unstimulated control regarding THY1 (magenta), PDPN (yellow), and DAPI (gray). (D) The expression of pro-inflammatory cytokine marker genes, (E) hypoxia-related and pro-angiogenic genes was studied via qPCR and normalized to the housekeeper gene *EF1A* (n=5). Data are shown as box plots (centerline, median; box limits, upper and lower quartiles; whiskers, maximum and minimum values). Statistics: Two-tailed Wilcoxon matched-pairs signed-rank test (A, B) and Mann-Whitney U test (D, E). P-values are indicated in the figure with *p <0.05 and **p <0.01.

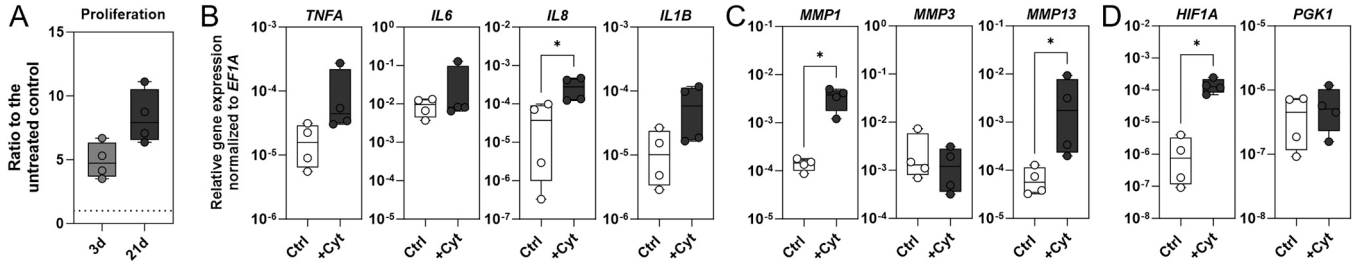

Fig. 9. Gene expression after long-term exposure to inflammatory stimuli. (A) BrdU assay was conducted to explore the proliferation rate of short- and long-term exposure as a ratio to the untreated control (n=4). (B) Expression of pro-inflammatory cytokine marker genes, (C) invasive, and (D) hypoxia-related was studied via qPCR and normalized to the housekeeper gene *EF1A* (n=4). Data are shown as box plots (centerline, median; box limits, upper and lower quartiles; whiskers, maximum and minimum values). Statistics: Wilcoxon Signed Rank Test compared to the control (A); Mann-Whitney U test (A-C); p-values are indicated in the graphs with *p <0.05.

indistinguishable in terms of plastic adherence, the characteristic elongated, spindle-shaped morphology, and the presence of mesenchymal-specific markers, coupled with the absence of hematopoietic-specific markers. This observation is consistent with the findings of Ugurlu and Karaoz, who performed a comparative analysis between Wharton's jelly-derived MSCs and dermal FLSs (Lorenz et al., 2008a). Their study showed that the expression levels of important cellular markers differed only slightly in these cell types, indicating a high phenotypic similarity (Lorenz et al., 2008a). Although studies report that FLSs exhibit an MSC-like phenotype, it has also been observed that MSCs express markers commonly associated with FLSs, including collagen and vimentin (Damerau et al., 2022; Lorenz et al., 2008b). Moreover, the differentiation ability was traditionally used to distinguish FLSs from MSCs, with FLSs being the negative control (Brendel et al., 2005). Recent research revealed that FLSs from various tissues such as skin, bronchial, and synovium could differentiate into lineages of the mesenchyme – e.g., adipogenic and osteogenic (Brohem et al., 2013b; Chen et al., 2007; Damerau et al., 2022; Sabatini et al., 2005a, 2005b). However, a clear distinction between these cell types remains elusive as no specific marker exists (Dominici et al., 2006; Lin et al., 2013). Therefore, it is unclear whether the characterized cells are MSC or synovial fibroblasts. The metabolic robustness of cells is significantly influenced by a number of factors, including the age and health status of the donor, and the precise conditions used for cell culture and expansion in an *in vitro* environment. Studies have shown that the nutrient-rich environment typical of *in vitro* cultures leads to a metabolic shift in MSCs that directs their dependence on energy production more towards OXPHOS (Pattappa et al., 2011; Yuan et al., 2019). In this study, we newly present comparative analyses between trauma-FLSs and MSCs, both exposed to a nutrient-rich *in vitro* culture environment. Our results show that under such conditions, MSCs preferentially utilize OXPHOS for energy production, in contrast to trauma-FLSs. Different metabolic orientations emphasize the intrinsic cellular adaptability to environmental factors and highlight the importance of metabolic pathways for cell function and therapeutic potential, which needs to be further explored.

Moreover, studies reported that adding CTGF promotes MSC differentiation into FLSs, at least regarding markers such as *COL1, COL3, FN1, FSP1,* and *TNC* (Lee et al., 2006, 2010a; Xu et al., 2015, 2017). As described by Lee et al., recombinant CTGF was used at a concentration of 100 ng/mL in combination with 50 µg/mL ascorbic acid (Lee et al., 2010b). Considering the pathways leading to fibroblast formation, FGF and IGF were used as potential inducers of fibroblastic differentiation at concentrations referring to Hegner et al. and Han et al. (Han et al., 2011;

Hegner et al., 2016). Here, we found no significant differences compared to CTGF stimulation alone. Our unbiased global proteome analysis showed that fibroblast markers such as COL1A1, COL1A2, and COL1A3 tended to be reduced by CTGF, while features such as VIM, FN1, FSP1, TNC, and DCN remained unchanged. In this regard, the expression of the classical marker vimentin was significantly higher in OA-FLS compared to MSCs, but unchanged at the gene level. Activated fibroblasts and myofibroblasts are the leading producers of structural proteins of the ECM (Karsdal et al., 2017). In this line, induced COL4 and COL6 expression is a driver and biomarker in fibrosis associated with pro-fibrotic myofibroblasts (Mak and Mei, 2017; Naugle et al., 2006; Williams et al., 2021). The primary function of FLSs is to synthesize ECM components, predominantly hyaluronan, primarily regulated by HAS2, as delineated by Caon et al. (Caon et al., 2021). The upregulation of HAS2 by CTGF stimulation suggests the improved ability to synthesize hyaluronic acid. This expression is not comparable to fibroblasts from trauma and OA patients but was observed in myofibroblasts induced by TGF-β1 (Evanko et al., 2015). In addition, overexpression of HAS is associated with fibroblast invasiveness, which promotes fibrosis (Li et al., 2016). CTGF also induced the expression of LOXL4, an indicator of fibrosis that correlates with tissue stiffness (Perryman and Gray, 2022). Interestingly, Elsafadi et al. identified *SERPINB2* as a gene repressed by TGF-β, whereas CTGF tended to induce it at the protein level (Lee et al., 2018). FN is a circulating protein component of the ECM that is readily degraded into fragments. Carnemolla et al. (Carnemolla et al., 1984) and Chevalier et al. (Chevalier, 1993) reported that elevated levels of FN fragments have been detected in the synovial fluid OA and RA patients. In contrast to studies indicating increased levels of FN in the synovial fluid and cartilage, our results show a significantly reduced *FN1* expression in OA-FLS compared to MSCs and trauma-FLSs. This observation is in line with our previous data showing a significantly reduced expression of FN1 in OA-FLSs at the protein level (Damerau et al., 2022). It is known that FLSs display characteristic gene expression patterns depending on their origin (Rinn et al., 2006). However, our data showed that MSCs are a suitable cell source to mimic the healthy synovial membrane *in vitro,* as MSCs and FLSs are phenotypically indistinguishable (Denu et al., 2016a). For developing healthy synovial membrane models, MSCs are better suited than CTGF-differentiated MSCs.

During inflammatory joint diseases, activated FLSs of the synovial membrane have been identified as critical drivers of persistent inflammation and cartilage degradation. However, profound insights into the pathogenic mechanisms and the impact of FLSs in the early stages of cartilage degradation are still limited. To study processes that occur in the synovium during rheumatic diseases, various *in vitro* alternative approaches to mimic the synovial membrane have been developed to overcome the current limitations of experiments using phylogenetically distant species (e.g., rodents) and break the translation barrier. A pioneering study by Kiener et al. used primary FLSs from RA patients to generate a 3D synovial membrane micromass (Kiener et al., 2006). They demonstrated that RA-FLSs when suspended in an ice-cold Matrigel™ matrix, can form a lining layer architecture at the interface between the matrix and liquid phase (Kiener et al., 2006). The extension of this model by including monocytes further demonstrated that RA-FLSs promote monocyte survival and accumulation in the lining layer (Broeren et al., 2019; Kiener et al., 2010). However, such models that rely on RA-FLS and animal-derived Matrigel™ do not represent the "healthy" state of the synovial membrane. Compared to standard static culture conditions, on-a-chip approaches have been demonstrated to better resemble the biochemical environment as well as mechanical forces that occur within the joint (Ong et al., 2023; Zou et al., 2022). Mimicking joint movement through mechanical stress in cartilage constructs contributed to cartilage matrix maintenance and is observed to slow the progression of OA (Ong et al., 2023). Mondadori and colleagues designed a microfluidic chip including synovial and chondral compartment to recapitulate the extravasation of monocytes to the synovium under perfused conditions (Mondadori et al., 2021). Moreover, Krebs et al. developed a microfluidic synovial chip platform to analyze the frequency of specific cell surface marker within synovial fluid aspirates (Krebs et al., 2017). The organoid-on-a-chip for joints developed to date can be divided into four main categories: Modeling inflammation, recapitulating immune responses, simulating mechanical forces, and studying genetic predisposition (Li et al., 2023). The study presented here aimed to simulate the geometry of the synovial membrane on the basis of MSCs. Therefore, MSCs were embedded in a synthetic hydrogel and, in contrast to a major part of previous studies, cultured under xeno-free conditions (Broeren et al., 2019; Kiener et al., 2006, 2010). Synthetic hydrogels possess desirable features for tissue engineering can be precisely tailored through chemical modifications (Samvelyan et al., 2021). For instance, incorporating chondrogenic molecules, such as biotinylated TGF-β3, facilitated the delivery of these molecules to cells embedded within the hydrogel. This process promoted the collagen type II expression and enhanced chondrogenesis (Stüdle et al., 2018). In our study, the synthetic hydrogel was modified with RGD sequences to enable the formation of a synovial lining layer. During the cultivation period, the cells formed a synovial lining structure consisting of two to four layers of viable cells, as described for the native synovial membrane (Smith, 2011). The synovial membrane model was incubated in a trans-well system to enable future stimulation with cytokines from basal and application of immune cells from apical. We demonstrated immune cell migration through the hydrogel and the trans-well system. Short- and long-term exposure to TNF-α, IL-6, and MIF in pathophysiological concentrations showed that pro-inflammatory effects could be studied in the animal-free synovial membrane model. In addition to the master cytokines TNF-α and IL-6, which essentially trigger inflammation in RA, they are also associated with OA pathology (Akeson and Malemud, 2017; Nishimoto et al., 2000; Yu et al., 2018). TNF-α promotes the expression and secretion of IL-6 and IL-8, which contribute to RA synovitis (Broeren et al., 2019; Mueller et al., 2010; Namba et al., 2017; Tanabe et al., 2010). Namba et al. investigated dogs' mitogen-activated protein kinase (MAPK) signaling pathway in synovial fibroblasts. They showed that TNF-α induced the IL-8 secretion and expression time-dependent (Namba et al., 2017). In this line, MAPK pathways have been found to upregulate the expression of MMP1, MMP3, and MMP13 (Holvoet et al., 2003; Jia et al., 2019; Park et al., 2011). Our synovial membrane model resembles a significant induced *IL8* expression already after short-term exposure and the MMP expression after long-term exposure *in vitro*. While TNF-α induces the proliferation of synovial cells, IL-6 inhibits it in the presence of the soluble IL-6 receptor (sIL-6R) (Nishimoto et al., 2000). As reported by Broeren and colleagues for TNF-α, we could recreate pathogenic processes such as enhanced glycolysis and hyperproliferation of the synovial lining layer – a hallmark of RA (Broeren et al., 2019; Kiener et al., 2010; Koedderitzsch et al., 2021). This is a major advantage compared to studies using synovial biopsies or diseased cells in which hyperplasia has already occurred. However, in this study the proliferation rate was the measure of hyperplasia. Future studies should also consider a spatial histologic evaluation, which would be possible using synovial organoids. In addition, we observed a substantial increase in the expression of *VEGFA* and *HIF1A*, both generally activated by hypoxia. However, recent research revealed that TNF-α and MIF could induce HIF-1α expression under normoxic conditions (Gaber et al., 2011; Zhou and Brune, 2006). Moreover, cell-cell and cell-matrix interactions are crucial for enhancing the robustness and applicability of this platform. These interactions regulate many aspects of cell function, including proliferation, migration, and differentiation (Shao et al., 2024). Understanding these dynamics can lead to more accurate models of disease. In addition, mechanical properties like forces, pressure, and stiffness influence cell behavior, differentiation, and tissue formation (Damerau et al., 2024). Accurately mimicking the mechanical environment of musculoskeletal tissues can create more physiologically relevant models. Finally, utilizing stem cells, particularly MSCs, is vital due to their ability to differentiate into various cell types found in musculoskeletal tissues. This

enables the creation of complex, multi-cellular models that closely replicate *in vivo* conditions. In future applications, cell types such as macrophages will be incorporated to mimic the processes that occur during arthritis more closely. Although the available 3D models still face major challenges, our animal-free approach can serve as an alternative to animal experiments to (i) study basic mechanisms in RA and OA, (ii) identify targets, and (iii) test treatment strategies. This is the first animal-free *in vitro* 3D synovial membrane model to study cytokine-driven mechanisms.

5. Conclusion

The assumption that synovial fibroblasts are derived from mesenchymal cells has driven research on the differentiation capacity of MSCs towards fibroblastic cell lineages, which is of particular interest and highly relevant for the purpose of tissue engineering and regenerative medicine. This study aimed to explore this potential by comparing synovial fibroblasts from trauma patients with MSCs, focusing on the role of CTGF in mediating this transition and comparing it with OA-FLS. Our results show that human knee-derived FLS from trauma patients exhibit a stem cell-like phenotype similar to bone marrow-derived MSCs. We also demonstrate that stimulation with CTGF induces MSCs to differentiate into a fibrotic fibroblast phenotype, highlighting the potential of MSCs in the development of healthy and diseased *in vitro* tissues. Furthermore, our study illustrates the ability to mimic the geometry of the synovial membrane using a biocompatible, RGD-functionalized synthetic hydrogel that supports cell arrangement in a lining layer-like structure. While exposure to inflammatory stimuli may not fully replicate arthritis, the MSC-based model offers a controlled system to investigate key events observed in human arthritis. This research contributes to understanding synovial fibroblast origin and MSCs as an optimal cell source for *in vitro* tissue engineering in health and disease. The latter is of utmost importance if access to healthy and diseased synovial tissue samples is limited.

CRediT authorship contribution statement

Philipp Mertins: Writing – review & editing, Data curation. **Frank Buttgereit:** Writing – review & editing, Writing – original draft, Supervision, Project administration, Funding acquisition, Conceptualization. **Timo Gaber:** Writing – review & editing, Writing – original draft, Supervision, Project administration, Funding acquisition, Conceptualization. **Alexandra Damerau:** Writing – review & editing, Writing – original draft, Visualization, Validation, Project administration, Methodology, Investigation, Funding acquisition, Formal analysis, Data curation, Conceptualization. **Marieluise Kirchner:** Writing – review & editing, Validation, Methodology, Formal analysis, Data curation.

Declaration of Competing Interest

The authors declare that they have no known competing financial interests or personal relationships that could have appeared to influence the work reported in this paper.

Data Availability

Data will be made available on request.

Acknowledgments

This work was supported by set Foundation (grant number P-077) and Charité 3R| Replace – Reduce – Refine. The authors would like to thank the Tissue Harvesting Core Facility of the BIH Berlin and the Center of Musculoskeletal Surgery of the Charité – Universitätsmedizin Berlin for providing bone marrow and synovial tissue. Furthermore, A.D. was gratefully supported by the German Academic Scholarship Foundation (Studienstiftung des deutschen Volkes) and the Joachim Herz Foundation (Add-on Fellowship 2020). A.D., T.G., and F.B. are members of the Berlin-Brandenburg research platform BB3R and Charité 3R.

References

Ai, R., Laragione, T., Hammaker, D., Boyle, D.L., Wildberg, A., Maeshima, K., Palescandolo, E., Krishna, V., Pocalyko, D., Whitaker, J.W., Bai, Y., Nagpal, S., Bachman, K.E., Ainsworth, R.I., Wang, M., Ding, B., Gulko, P.S., Wang, W., Firestein, G.S., 2018. Comprehensive epigenetic landscape of rheumatoid arthritis fibroblast-like synoviocytes. Nat. Commun. 9, 1921-1921.

Akeson, G., Malemud, C.J., 2017. A role for soluble IL-6 receptor in osteoarthritis. J. Funct. Morphol. Kinesiol 2, 27.

de Almeida, Danilo C., Ferreira, Marcelo R.P., Franzen, J., Weidner, Carola I., Frobel, J., Zenke, M., Costa, Ivan G., Wagner, W., 2016. Epigenetic classification of human mesenchymal stromal cells. Stem Cell Rep. 6, 168–175.

Astarita, J.L., Acton, S.E., Turley, S.J., 2012. Podoplanin: emerging functions in development, the immune system, and cancer. Front. Immunol. 3, 283.

Balakrishnan, L., Nirujogi, R.S., Ahmad, S., Bhattacharjee, M., Manda, S.S., Renuse, S., Kelkar, D.S., Subbannayya, Y., Raju, R., Goel, R., Thomas, J.K., Kaur, N., Dhillon, M., Tankala, S.G., Jois, R., Vasdev, V., Ramachandra, Y., Sahasrabuddhe, N.A., Prasad Ts, K., Mohan, S., Gowda, H., Shankar, S., Pandey, A., 2014. Proteomic analysis of human osteoarthritis synovial fluid. Clin. Proteom. 11, 6.

Baymurat, A.C., Ozturk, A.M., Yetkin, H., Ergun, M.A., Helvacioglu, F., Ozkizilcik, A., Tuzlakoglu, K., Sener, E.E., Erdogan, D., 2015. Bio-engineered synovial membrane to prevent tendon adhesions in rabbit flexor tendon model. J. Biomed. Mater. Res. A 103, 84–90.

Bi, Y., Ehirchiou, D., Kilts, T.M., Inkson, C.A., Embree, M.C., Sonoyama, W., Li, L., Leet, A.I., Seo, B.M., Zhang, L., Shi, S., Young, M.F., 2007. Identification of tendon stem/progenitor cells and the role of the extracellular matrix in their niche. Nat. Med. 13, 1219–1227.

Blasi, A., Martino, C., Balducci, L., Saldarelli, M., Soleti, A., Navone, S.E., Canzi, L., Cristini, S., Invernici, G., Parati, E.A., Alessandri, G., 2011. Dermal fibroblasts display similar phenotypic and differentiation capacity to fat-derived mesenchymal stem cells, but differ in anti-inflammatory and angiogenic potential. Vasc. Cell 3, 5.

Bondeson, J., Wainwright, S.D., Lauder, S., Amos, N., Hughes, C.E., 2006. The role of synovial macrophages and macrophage-produced cytokines in driving aggrecanases, matrix metalloproteinases, and other destructive and inflammatory responses in osteoarthritis. Arthritis Res. Ther. 8, R187.

Bordignon, P., Bottoni, G., Xu, X., Popescu, A.S., Truan, Z., Guenova, E., Kofler, L., Jafari, P., Ostano, P., Rocken, M., Neel, V., Dotto, G.P., 2019. Dualism of FGF and TGF-beta signaling in heterogeneous cancer-associated fibroblast activation with ETV1 as a critical determinant. Cell Rep. 28, 2358–2372 e2356.

Brendel, C., Kuklick, L., Hartmann, O., Kim, T.D., Boudriot, U., Schwell, D., Neubauer, A., 2005. Distinct gene expression profile of human mesenchymal stem cells in comparison to skin fibroblasts employing cDNA microarray analysis of 9600 genes. Gene Expr. 12, 245–257.

Broeren, M.G.A., Waterborg, C.E.J., Wiegertjes, R., Thurlings, R.M., Koenders, M.I., Van Lent, P., Van der Kraan, P.M., Van de Loo, F.A.J., 2019. A three-dimensional model to study human synovial pathology. ALTEX 36, 18–28.

Brohem, C.A., de Carvalho, C.M., Radoski, C.L., Santi, F.C., Baptista, M.C., Swinka, B.B., de, A.U.C., de Araujo, L.R., Graf, R.M., Feferman, I.H., Lorencini, M., 2013b. Comparison between fibroblasts and mesenchymal stem cells derived from dermal and adipose tissue. Int. J. Cosmet. Sci. 35, 448–457.

Brohem, C.A., de Carvalho, C.M., Radoski, C.L., Santi, F.C., Baptista, M.C., Swinka, B.B., de, A., Urban, C., de Araujo, L.R.R., Graf, R.M., Feferman, I.H.S., Lorencini, M., 2013a. Comparison between fibroblasts and mesenchymal stem cells derived from dermal and adipose tissue, 35, 448–457.

Caon, I., Parnigoni, A., Viola, M., Karousou, E., Passi, A., Vigetti, D., 2021. Cell energy metabolism and hyaluronan synthesis. J. Histochem Cytochem 69, 35–47.

Cappellesso-Fleury, S., Puissant-Lubrano, B., Apoil, P.A., Titeux, M., Winterton, P., Casteilla, L., Bourin, P., Blancher, A., 2010. Human fibroblasts share immunosuppressive properties with bone marrow mesenchymal stem cells. J. Clin. Immunol. 30, 607–619.

Carnemolla, B., Cutolo, M., Castellani, P., Balza, E., Raffanti, S., Zardi, L., 1984. Characterization of synovial fluid fibronectin from patients with rheumatic inflammatory diseases and healthy subjects. Arthritis Rheum. 27, 913–921.

Chang, H.Y., Chi, J.T., Dudoit, S., Bondre, C., van de Rijn, M., Botstein, D., Brown, P.O., 2002. Diversity, topographic differentiation, and positional memory in human fibroblasts. Proc. Natl. Acad. Sci. USA 99, 12877–12882.

Chen, F.G., Zhang, W.J., Bi, D., Liu, W., Wei, X., Chen, F.F., Zhu, L., Cui, L., Cao, Y., 2007. Clonal analysis of nestin(-) vimentin(+) multipotent fibroblasts isolated from human dermis. J. Cell Sci. 120, 2875–2883.

Chevalier, X., 1993. Fibronectin, cartilage, and osteoarthritis. Semin Arthritis Rheum. 22, 307–318.

Damerau, A., Gaber, T., 2020. Modeling rheumatoid arthritis in vitro: from experimental feasibility to physiological proximity. Int. J. Mol. Sci.

Damerau, A., Kirchner, M., Pfeiffenberger, M., Ehlers, L., Do Nguyen, D.H., Mertins, P., Bartek, B., Maleitzke, T., Palmowski, Y., Hardt, S., Winkler, T., Buttgereit, F., Gaber, T., 2022. Metabolic reprogramming of synovial fibroblasts in osteoarthritis by inhibition of pathologically overexpressed pyruvate dehydrogenase kinases. Metab. Eng. 72, 116–132.

Damerau, A., Pfeiffenberger, M., Weber, M.C., Burmester, G.R., Buttgereit, F., Gaber, T., Lang, A., 2020. A human osteochondral tissue model mimicking cytokine-induced key features of arthritis in vitro. Int J. Mol. Sci. 22.
Damerau, A., Rosenow, E., Alkhoury, D., Buttgereit, F., Gaber, T., 2024. Fibrotic pathways and fibroblast-like synoviocyte phenotypes in osteoarthritis, 15.
Denu, R.A., Nemcek, S., Bloom, D.D., Goodrich, A.D., Kim, J., Mosher, D.F., Hematti, P., 2016b. Fibroblasts and mesenchymal stromal/stem cells are phenotypically indistinguishable. Acta Haematol. 136, 85–97.
Denu, R.A., Nemcek, S., Bloom, D.D., Goodrich, A.D., Kim, J., Mosher, D.F., Hematti, P., 2016a. Fibroblasts and mesenchymal stromal/stem cells are phenotypically indistinguishable. Acta Haematol. 136, 85–97.
Dominici, M., Le Blanc, K., Mueller, I., Slaper-Cortenbach, I., Marini, F., Krause, D., Deans, R., Keating, A., Prockop, D., Horwitz, E., 2006. Minimal criteria for defining multipotent mesenchymal stromal cells. The International Society for Cellular Therapy position statement. Cytotherapy 8, 315–317.
Evanko, S.P., Potter-Perigo, S., Petty, L.J., Workman, G.A., Wight, T.N., 2015. Hyaluronan controls the deposition of fibronectin and collagen and modulates TGF-beta1 induction of lung myofibroblasts. Matrix Biol. 42, 74–92.
Fan, H., Liu, H., Toh, S.L., Goh, J.C.H., 2008. Enhanced differentiation of mesenchymal stem cells co-cultured with ligament fibroblasts on gelatin/silk fibroin hybrid scaffold. Biomaterials 29, 1017–1027.
Firestein, G.S., McInnes, I.B., 2017. Immunopathogenesis of rheumatoid arthritis. Immunity 46, 183–196.
Gaber, T., Schellmann, S., Erekul, K.B., Fangradt, M., Tykwinska, K., Hahne, M., Maschmeyer, P., Wagegg, M., Stahn, C., Kolar, P., Dziurla, R., Löhning, M., Burmester, G.R., Buttgereit, F., 2011. Macrophage migration inhibitory factor counterregulates dexamethasone-mediated suppression of hypoxia-inducible factor-1 alpha function and differentially influences human CD4+ T cell proliferation under hypoxia. J. Immunol. (Baltim. Md. 1950) 186, 764–774.
Ge, X., Frank-Bertoncelj, M., Klein, K., McGovern, A., Kuret, T., Houtman, M., Burja, B., Micheroli, R., Shi, C., Marks, M., Filer, A., Buckley, C.D., Orozco, G., Distler, O., Morris, A.P., Martin, P., Eyre, S., Ospelt, C., 2021. Functional genomics atlas of synovial fibroblasts defining rheumatoid arthritis heritability. Genome Biol. 22, 247.
Ghahremani-Nasab, M., Del Bakhshayesh, A.R., Akbari-Gharalari, N., Mehdipour, A., 2023. Biomolecular and cellular effects in skin wound healing: the association between ascorbic acid and hypoxia-induced factor. J. Biol. Eng. 17, 62.
Goodpaster, T., Legesse-Miller, A., Hameed, M.R., Aisner, S.C., Randolph-Habecker, J., Coller, H.A., 2007. An immunohistochemical method for identifying fibroblasts in formalin-fixed, paraffin-embedded tissue. J. Histochem. Cytochem. 56, 347–358.
Han, Y., Chai, J., Sun, T., Li, D., Tao, R., 2011. Differentiation of human umbilical cord mesenchymal stem cells into dermal fibroblasts in vitro. Biochem. Biophys. Res. Commun. 413, 561–565.
Hegner, B., Schaub, T., Catar, R., Kusch, A., Wagner, P., Essin, K., Lange, C., Riemekasten, G., Dragun, D., 2016. Intrinsic deregulation of vascular smooth muscle and myofibroblast differentiation in mesenchymal stromal cells from patients with systemic sclerosis. PLoS One 11, e0153101.
Holvoet, S., Vincent, C., Schmitt, D., Serres, M., 2003. The inhibition of MAPK pathway is correlated with down-regulation of MMP-9 secretion induced by TNF-α in human keratinocytes. Exp. Cell Res. 290, 108–119.
Huber, L.C., Distler, O., Tarner, I., Gay, R.E., Gay, S., Pap, T., 2006. Synovial fibroblasts: key players in rheumatoid arthritis. Rheumatol. (Oxf., Engl.) 45, 669–675.
Iwano, M., Plieth, D., Danoff, T.M., Xue, C., Okada, H., Neilson, E.G., 2002. Evidence that fibroblasts derive from epithelium during tissue fibrosis. J. Clin. Invest 110, 341–350.
Jia, Y.-L., Liu, X.-J., Wen, H., Zhan, Y.-P., Xiang, M.-H., 2019. The expression of MAPK signaling pathways in conjunctivochalasis. Int J. Ophthalmol. 12, 1801–1806.
Jiang, D., Guo, R., Machens, H.G., Rinkevich, Y., 2023. Diversity of fibroblasts and their roles in wound healing. Cold Spring Harb. Perspect. Biol. 15.
Karonitsch, T., Beckmann, D., Dalwigk, K., Niederreiter, B., Studenic, P., Byrne, R.A., Holinka, J., Sevelda, F., Korb-Pap, A., Steiner, G., Smolen, J.S., Pap, T., Kiener, H.P., 2017. Targeted inhibition of Janus kinases abates interfon gamma-induced invasive behaviour of fibroblast-like synoviocytes. Rheumatology 57, 572–577.
Karsdal, M.A., Nielsen, S.H., Leeming, D.J., Langholm, L.L., Nielsen, M.J., Manon-Jensen, T., Siebuhr, A., Gudmann, N.S., Rønnow, S., Sand, J.M., Daniels, S.J., Mortensen, J.H., Schuppan, D., 2017. The good and the bad collagens of fibrosis – their role in signaling and organ function. Adv. Drug Deliv. Rev. 121, 43–56.
Kiener, H.P., Lee, D.M., Agarwal, S.K., Brenner, M.B., 2006. Cadherin-11 induces rheumatoid arthritis fibroblast-like synoviocytes to form lining layers in vitro. Am. J. Pathol. 168, 1486–1499.
Kiener, H.P., Watts, G.F., Cui, Y., Wright, J., Thornhill, T.S., Skold, M., Behar, S.M., Niederreiter, B., Lu, J., Cernadas, M., Coyle, A.J., Sims, G.P., Smolen, J., Warman, M. L., Brenner, M.B., Lee, D.M., 2010. Synovial fibroblasts self-direct multicellular lining architecture and synthetic function in three-dimensional organ culture. Arthritis Rheum. 62, 742–752.
Koedderitzsch, K., Zezina, E., Li, L., Herrmann, M., Biesemann, N., 2021. TNF induces glycolytic shift in fibroblast like synoviocytes via GLUT1 and HIF1A. Sci. Rep. 11, 19385.
Krebs, J.C., Alapan, Y., Dennstedt, B.A., Wera, G.D., Gurkan, U.A., 2017. Microfluidic processing of synovial fluid for cytological analysis. Biomed. Micro 19, 20.
Lee, N.-H., Cho, A., Park, S.-R., Lee, J.W., Sung Taek, P., Park, C.H., Choi, Y.-H., Lim, S., Baek, M.-K., Kim, D.Y., Jin, M., Lee, H.-Y., Hong, I.-S., 2018. SERPINB2 is a novel indicator of stem cell toxicity. Cell Death Dis. 9, 724.
Lee, C.H., Moioli, E.K., Mao, J.J., 2006. Fibroblastic differentiation of human mesenchymal stem cells using connective tissue growth factor. Conf Proc IEEE Eng Med Biol Soc 2006, 775-778.
Lee, C.H., Shah, B., Moioli, E.K., Mao, J.J., 2010a. CTGF directs fibroblast differentiation from human mesenchymal stem/stromal cells and defines connective tissue healing in a rodent injury model. J. Clin. Investig. 120, 3340–3349.
Lee, C.H., Shah, B., Moioli, E.K., Mao, J.J., 2010b. CTGF directs fibroblast differentiation from human mesenchymal stem/stromal cells and defines connective tissue healing in a rodent injury model. J. Clin. Invest 120, 3340–3349.
Lendahl, U., Muhl, L., Betsholtz, C., 2022. Identification, discrimination and heterogeneity of fibroblasts. Nat. Commun. 13, 3409.
Li, Y., Liang, J., Yang, T., Monterrosa Mena, J., Huan, C., Xie, T., Kurkciyan, A., Liu, N., Jiang, D., Noble, P.W., 2016. Hyaluronan synthase 2 regulates fibroblast senescence in pulmonary fibrosis. Matrix Biol. 55, 35–48.
Li, Y., Liu, Z., Jin, Y., Zhu, X., Wang, S., Yang, J., Ren, Y., Fu, Q., Xiong, H., Zou, G., Liu, Y., 2017. Differentiation of human amniotic mesenchymal stem cells into human anterior cruciate ligament fibroblast cells by in vitro coculture. Biomed. Res. Int. 2017, 7360354.
Li, Z.A., Sant, S., Cho, S.K., Goodman, S.B., Bunnell, B.A., Tuan, R.S., Gold, M.S., Lin, H., 2023. Synovial joint-on-a-chip for modeling arthritis: progress, pitfalls, and potential. Trends Biotechnol. 41, 511–527.
Lin, C.-S., Xin, Z.-C., Dai, J., Lue, T.F., 2013. Commonly used mesenchymal stem cell markers and tracking labels: Limitations and challenges. Histol. Histopathol. 28, 1109–1116.
Lorenz, K., Sicker, M., Schmelzer, E., Rupf, T., Salvetter, J., Schulz-Siegmund, M., Bader, A., 2008a. Multilineage differentiation potential of human dermal skin-derived fibroblasts, 17, 925–932.
Lorenz, K., Sicker, M., Schmelzer, E., Rupf, T., Salvetter, J., Schulz-Siegmund, M., Bader, A., 2008b. Multilineage differentiation potential of human dermal skin-derived fibroblasts. Exp. Dermatol. 17, 925–932.
Lv, F.J., Tuan, R.S., Cheung, K.M., Leung, V.Y., 2014. Concise review: the surface markers and identity of human mesenchymal stem cells. Stem Cells 32, 1408–1419.
Mak, K.M., Mei, R., 2017. Basement membrane type IV collagen and laminin: an overview of their biology and value as fibrosis biomarkers of liver disease. Anat. Rec. (Hoboken N. J. 2007) 300, 1371–1390.
Matsuo, Y., Saito, T., Yamamoto, A., Kohsaka, H., 2018. Origins of fibroblasts in rheumatoid synovial tissues: Implications from organ fibrotic models. Mod. Rheuma 28, 579–582.
McAnulty, R.J., 2007. Fibroblasts and myofibroblasts: their source, function and role in disease. Int. J. Biochem. Cell Biol. 39, 666–671.
Mizoguchi, F., Slowikowski, K., Wei, K., Marshall, J.L., Rao, D.A., Chang, S.K., Nguyen, H.N., Noss, E.H., Turner, J.D., Earp, B.E., Blazar, P.E., Wright, J., Simmons, B.P., Donlin, L.T., Kalliolias, G.D., Goodman, S.M., Bykerk, V.P., Ivashkiv, L.B., Lederer, J.A., Hacohen, N., Nigrovic, P.A., Filer, A., Buckley, C.D., Raychaudhuri, S., Brenner, M.B., 2018. Functionally distinct disease-associated fibroblast subsets in rheumatoid arthritis. Nat. Commun. 9, 789.
Mondadori, C., Palombella, S., Salehi, S., Talò, G., Visone, R., Rasponi, M., Redaelli, A., Sansone, V., Moretti, M., Lopa, S., 2021. Recapitulating monocyte extravasation to the synovium in an organotypic microfluidic model of the articular joint. Biofabrication 13.
Moreau, J.E., Chen, J., Bramono, D.S., Volloch, V., Chernoff, H., Vunjak-Novakovic, G., Richmond, J.C., Kaplan, D.L., Altman, G.H., 2005. Growth factor induced fibroblast differentiation from human bone marrow stromal cells in vitro. J. Orthop. Res. 23, 164–174.
Mueller, L., von Seggern, L., Schumacher, J., Goumas, F., Wilms, C., Braun, F., Broering, D.C., 2010. TNF-alpha similarly induces IL-6 and MCP-1 in fibroblasts from colorectal liver metastases and normal liver fibroblasts. Biochem Biophys. Res. Commun. 397, 586–591.
Namba, S., Nakano, R., Kitanaka, T., Kitanaka, N., Nakayama, T., Sugiya, H., 2017. ERK2 and JNK1 contribute to TNF-alpha-induced IL-8 expression in synovial fibroblasts. PLoS One 12, e0182923.
Naugle, J.E., Olson, E.R., Zhang, X., Mase, S.E., Pilati, C.F., Maron, M.B., Folkesson, H.G., Horne, W.I., Doane, K.J., Meszaros, J.G., 2006. Type VI collagen induces cardiac myofibroblast differentiation: implications for postinfarction remodeling. Am. J. Physiol. Heart Circ. Physiol. 290, H323–330.
Nishimoto, N., Ito, A., Ono, M., Tagoh, H., Matsumoto, T., Tomita, T., Ochi, T., Yoshizaki, K., 2000. IL-6 inhibits the proliferation of fibroblastic synovial cells from rheumatoid arthritis patients in the presence of soluble IL-6 receptor. Int. Immunol. 12, 187–193.
Ong, L.J.Y., Fan, X., Rujia Sun, A., Mei, L., Toh, Y.C., Prasadam, I., 2023. Controlling microenvironments with organs-on-chips for osteoarthritis modelling. Cells 12.
Orr, C., Vieira-Sousa, E., Boyle, D.L., Buch, M.H., Buckley, C.D., Canete, J.D., Catrina, A. I., Choy, E.H.S., Emery, P., Fearon, U., Filer, A., Gerlag, D., Humby, F., Isaacs, J.D., Just, S.A., Lauwerys, B.R., Le Goff, B., Manzo, A., McGarry, T., McInnes, I.B., Najm, A., Pitzalis, C., Pratt, A., Smith, M., Tak, P.P., Thurlings, R., Fonseca, J.E., Veale, D.J., Tas, S.W., 2017. Synovial tissue research: a state-of-the-art review. Nat. Rev. Rheuma 13, 463–475.
Park, S., Jung, H.H., Park, Y.H., Ahn, J.S., Im, Y.-H., 2011. ERK/MAPK pathways play critical roles in EGFR ligands-induced MMP1 expression. Biochem. Biophys. Res. Commun. 407, 680–686.
Pattappa, G., Heywood, H.K., de Bruijn, J.D., Lee, D.A., 2011. The metabolism of human mesenchymal stem cells during proliferation and differentiation. J. Cell. Physiol. 226, 2562–2570.
Perryman, L., Gray, S.G., 2022. Fibrosis in mesothelioma: potential role of lysyl oxidases. Cancers (Basel) 14, 981.
Plikus, M.V., Wang, X., Sinha, S., Forte, E., Thompson, S.M., Herzog, E.L., Driskell, R.R., Rosenthal, N., Biernaskie, J., Horsley, V., 2021. Fibroblasts: origins, definitions, and functions in health and disease. Cell 184, 3852–3872.

Rhee, D.K., Marcelino, J., Baker, M., Gong, Y., Smits, P., Lefebvre, V., Jay, G.D., Stewart, M., Wang, H., Warman, M.L., Carpten, J.D., 2005. The secreted glycoprotein lubricin protects cartilage surfaces and inhibits synovial cell overgrowth. J. Clin. Invest. 115, 622–631.
Rinn, J.L., Bondre, C., Gladstone, H.B., Brown, P.O., Chang, H.Y., 2006. Anatomic demarcation by positional variation in fibroblast gene expression programs. PLoS Genet. 2, e119.
Sabatini, F., Petecchia, L., Tavian, M., Jodon de Villeroché, V., Rossi, G.A., Brouty-Boyé, D., 2005b. Human bronchial fibroblasts exhibit a mesenchymal stem cell phenotype and multilineage differentiating potentialities. Lab. Investig. J. Tech. Methods Pathol. 85, 962–971.
Sabatini, F., Petecchia, L., Tavian, M., de Villeroché, V.J., Rossi, G.A., Brouty-Boyé, D., 2005a. Human bronchial fibroblasts exhibit a mesenchymal stem cell phenotype and multilineage differentiating potentialities. Lab. Investig. 85, 962–971.
Samvelyan, H.J., Hughes, D., Stevens, C., Staines, K.A., 2021. Models of osteoarthritis: relevance and new insights. Calcif. Tissue Int. 109, 243–256.
Scanzello, C.R., Goldring, S.R., 2012. The role of synovitis in osteoarthritis pathogenesis. Bone 51, 249–257.
Shao, Z., Wang, B., Gao, H., Zhang, S., 2024. Microenvironmental interference with intra-articular stem cell regeneration influences the onset and progression of arthritis. Front Genet 15, 1380696.
Shen, J., Abu-Amer, Y., O'Keefe, R.J., McAlinden, A., 2017. Inflammation and epigenetic regulation in osteoarthritis. Connect Tissue Res. 58, 49–63.
Smith, M.D., 2011. The normal synovium. Open Rheuma J. 5, 100–106.
Smith, M.H., Gao, V.R., Periyakoil, P.K., Kochen, A., DiCarlo, E.F., Goodman, S.M., Norman, T.M., Donlin, L.T., Leslie, C.S., Rudensky, A.Y., 2023. Drivers of heterogeneity in synovial fibroblasts in rheumatoid arthritis. Nat. Immunol. 24, 1200–1210.
Smolen, J.S., Aletaha, D., Barton, A., Burmester, G.R., Emery, P., Firestein, G.S., Kavanaugh, A., McInnes, I.B., Solomon, D.H., Strand, V., Yamamoto, K., 2018. Rheumatoid arthritis. Nat. Rev. Dis. Prim. 4, 18001.
Soundararajan, M., Kannan, S., 2018. Fibroblasts and mesenchymal stem cells: two sides of the same coin? J. Cell Physiol. 233, 9099–9109.
Stüdle, C., Vallmajó-Martín, Q., Haumer, A., Guerrero, J., Centola, M., Mehrkens, A., Schaefer, D.J., Ehrbar, M., Barbero, A., Martin, I., 2018. Spatially confined induction of endochondral ossification by functionalized hydrogels for ectopic engineering of osteochondral tissues. Biomaterials 171, 219–229.
Tanabe, K., Matsushima-Nishiwaki, R., Yamaguchi, S., Iida, H., Dohi, S., Kozawa, O., 2010. Mechanisms of tumor necrosis factor-α-induced interleukin-6 synthesis in glioma cells. J. Neuroinflamm. 7, 16.
Tong, Z., Sant, S., Khademhosseini, A., Jia, X., 2011. Controlling the fibroblastic differentiation of mesenchymal stem cells via the combination of fibrous scaffolds and connective tissue growth factor. Tissue Eng. Part A 17, 2773–2785.
Ulukan, B., Sila Ozkaya, Y., Zeybel, M., 2019. Advances in the epigenetics of fibroblast biology and fibrotic diseases. Curr. Opin. Pharmacol. 49, 102–109.
Williams, L., Layton, T., Yang, N., Feldmann, M., Nanchahal, J., 2021. Collagen VI as a driver and disease biomarker in human fibrosis. FEBS J.
Xu, R., Taskin, M.B., Rubert, M., Seliktar, D., Besenbacher, F., Chen, M., 2015. hiPS-MSCs differentiation towards fibroblasts on a 3D ECM mimicking scaffold. Sci. Rep. 5, 8480.
Xu, R., Zhao, H., Muhammad, H., Dong, M., Besenbacher, F., Chen, M., 2017. Dual-delivery of FGF-2/CTGF from Silk Fibroin/PLCL-PEO coaxial fibers enhances MSC proliferation and fibrogenesis. Sci. Rep. 7, 8509.
Yoon, D., Yoon, D., Sim, H., Hwang, I., Lee, J.S., Chun, W., 2018. Accelerated wound healing by fibroblasts differentiated from human embryonic stem cell-derived mesenchymal stem cells in a pressure ulcer animal model. Stem Cells Int 2018, 4789568.
Yu, F.Y., Xie, C.Q., Jiang, C.L., Sun, J.T., Huang, X.W., 2018. TNF-α increases inflammatory factor expression in synovial fibroblasts through the toll-like receptor-3-mediated ERK/AKT signaling pathway in a mouse model of rheumatoid arthritis. Mol. Med. Rep. 17, 8475–8483.
Yuan, X., Logan, T.M., Ma, T., 2019. Metabolism in human mesenchymal stromal cells: a missing link between hMSC Biomanufacturing and Therapy?, 10.
Zeisberg, M., Kalluri, R., 2004. The role of epithelial-to-mesenchymal transition in renal fibrosis. J. Mol. Med. (Berl. Ger.) 82, 175–181.
Zhou, J., Brune, B., 2006. Cytokines and hormones in the regulation of hypoxia inducible factor-1alpha (HIF-1alpha). Cardiovasc Hematol. Agents Med. Chem. 4, 189–197.
Zou, Z., Luo, X., Chen, Z., Zhang, Y.S., Wen, C., 2022. Emerging microfluidics-enabled platforms for osteoarthritis management: from benchtop to bedside. Theranostics 12, 891–909.